THE ASTROPHYSICAL JOURNAL, 420:87–109, 1994 January 1

H II REGIONS AND THE ABUNDANCE PROPERTIES OF SPIRAL GALAXIES[1]

DENNIS ZARITSKY[2]
Carnegie Observatories, 813 Santa Barbara Street, Pasadena, CA 91101-1292. E-mail: dennis@ociw.edu
ROBERT C. KENNICUTT, JR.
Steward Observatory, University of Arizona, Tucson, AZ 85721. E-mail: robk@as.arizona.edu
AND
JOHN P. HUCHRA
Harvard-Smithsonian Center for Astrophysics, 60 Garden Street, Cambridge, MA 02138. E-mail: huchra@cfa.harvard.edu
Received 1993 May 12; accepted 1993 July 13

ABSTRACT

We investigate the relationships between the characteristic oxygen abundance, the radial abundance gradient, and the macroscopic properties of spiral galaxies by examining the properties of individual H II regions within those galaxies. Our observations of the line flux ratio ([O II] $\lambda\lambda$3726, 3729 + [O III] $\lambda\lambda$4959, 5007)/Hβ for 159 H II regions in 14 spiral galaxies are combined with published data to provide a sample of 39 disk galaxies for which ([O II] + [O III])/Hβ has been measured for at least five H II regions. We find that the characteristic gas-phase abundances and luminosities of spiral galaxies are strongly correlated. This relationship maps almost directly onto the luminosity-metallicity relationship of irregular galaxies and is also quite similar to that found for elliptical and dwarf spheroidal galaxies. Within our sample of spirals, a strong correlation between characteristic abundance and Hubble type also exists. The correlation between luminosity and Hubble type complicates the issue, but we discuss several interpretations of the correlations. The relationship between circular velocity and characteristic abundance is also discussed. We find that the slopes of the radial abundance gradients, when expressed in units of dex/isophotal radius, do not significantly correlate with either luminosity or Hubble type. However, the hypothesis that both early and very late type spirals have shallower gradients than intermediate spirals is consistent with the data. We find suggestive evidence that the presence of a bar induces a flatter gradient and also briefly discuss whether abundance gradients are exponential, as is usually assumed.

We investigate the properties of individual H II regions in a subset of 42 regions for which we have spectra that cover almost the entire spectral range from 3500 to 9800 Å. We use those data to estimate the densities and ionizing spectra within the H II regions. We confirm that the ionizing spectrum hardens with increasing radius and decreasing abundance. We find no correlation between the ionization parameter and either radius or abundance, but this may be due to significant scatter introduced by the simple conversion of line ratios to ionization parameter.

Subject headings: galaxies: abundances — galaxies: spiral — H II regions

1. INTRODUCTION

We can improve our understanding of galaxy formation and evolution by testing the predictions from various chemical evolution models against observations. The chemical composition of stars and gas within a galaxy depend on the local initial composition, star formation history, gas infall and outflow, stellar yields, and initial mass function. Although it is difficult to disentangle the effects of the various contributors, measurements of current elemental abundances constrain the myriad of possible evolutionary histories of the existing stars and gas.

The measurement of the distribution of elemental abundances within galaxies is one step along a sequence that may enable us to understand galaxy formation and evolution. In this investigation we confine ourselves to the study of oxygen in disk galaxies. We consider the "first" and "second" moments of the oxygen abundance distribution in disks, namely the mean, or characteristic, abundance and the radial abundance gradient. Beginning with studies by Searle (1971) and Shields (1974), many have investigated the topics of H II region elemental abundances and the distribution of oxygen within spiral galaxy disks. Pagel and coworkers made progress in calibrating line ratios and constructing temperature and ionization parameter diagnostics (see Edmunds & Pagel 1984, hereafter EP; Vílchez & Pagel 1988). Others obtained large observational samples with which to study the properties of H II regions (see McCall, Rybski, & Shields 1985, hereafter MRS). Until the recent study by Vila-Costas & Edmunds (1992, hereafter VE), the properties of H II regions in spiral galaxies had been linked to local properties such as local surface density (see EP) much more convincingly than to global properties such as luminosity or Hubble type. With the larger sample of galaxies now available, we can further examine the relationships between the chemical properties of spiral galaxies and their macroscopic properties. Whatever relationships are found can then serve as constraints on models of galaxy formation and evolution.

[1] This work is based in part on observations carried out at the Multiple Mirror Telescope Observatory, a joint facility of the University of Arizona and the Smithsonian Institution.
[2] Hubble Fellow.

There have been several investigations of possible relationships between the global abundance properties of galaxies and their structural characteristics. However, the small number of galaxies studied and the small number of H II regions studied per galaxy precluded definitive conclusions. For example, it remains unclear whether the characteristic abundance of a spiral galaxy is determined by its Hubble type (as suggested by Smith 1975 and EP) or by its luminosity (as advocated by Garnett & Shields 1987). Possibly, both factors are important. VE made significant progress in this area by compiling and analyzing data from many sources.

In this paper we combine new observations of 159 H II regions in 14 galaxies with existing data in the literature to study the abundance distributions in a sample of 39 disk galaxies. One difficulty in developing comparison samples has been that early-type spirals, which have much fainter H II regions than do late-type galaxies, are underrepresented in available samples. Oey & Kennicutt (1993, hereafter OK) alleviated this imbalance by measuring spectra of 67 H II regions in early-type spirals. By combining our sample of observations, which enlarges the available sample of late-type spirals, the OK sample of early-type spirals, and other published observations, we obtain an extensive and representative sample with which to examine relationships between the global abundance properties and the macroscopic properties of galaxies.

One difference between our study and those of VE and OK is our emphasis on only using galaxies that have at least five observed H II regions. Correspondingly, we discuss below the relative uncertainties inherent in the measurement of the characteristic abundance and abundance gradient as a function of the number of H II regions observed per galaxy. In previous studies, mean abundances and abundance gradients are usually measured using fewer than 10 regions per galaxy, and often fewer than five. We wish to significantly enlarge the number of H II regions in relatively well-sampled ($\geq$five observed regions) spiral galaxies for which [O II], [O III], and Hβ are measured.

The motivation for such work is to enhance our understanding of galaxy evolution. Observational work on both elliptical and spiral galaxies is now progressing well. For ellipticals, the structural parameters are known to be related through the fundamental plane relationships (Dressler et al. 1987; Djorgovski & Davis 1987; Bender, Burstein, & Faber 1992), and abundances have been related to both global properties (Faber 1973; Brodie & Huchra 1991; Bender, Burstein, & Faber 1993) and local properties (Franx & Illingworth 1990). Although the tight correlations found for ellipticals are not yet fully understood, they place demanding constraints on models of elliptical formation. Spirals are in some sense more complicated systems because they are actively evolving. However, with the work presented in VE and here, we can address questions that are analogous to those posed for ellipticals. Principally, are the abundances of spirals related to properties of the galaxies themselves or only to those of the local interstellar medium? Do the properties of spirals depend on only a few parameters?

The paper is organized as follows. Our observations and reductions are described in § 2. Various observed line ratios and their implications for the properties of individual H II regions are discussed in § 3. The relationships between the abundances, abundance gradients, and other properties of galaxies are discussed in § 4. Several of our observational results confirm those found independently by VE, and we will compare our respective results.

2. OBSERVATIONS AND DATA REDUCTION

2.1. *The Galaxy Sample*

An original motivation for our survey was the need to measure abundances for Cepheid variable target fields in the *HST* extragalactic distance scale key project. The selection criteria for the key project satisfies many of the criteria that are useful for the abundance project (i.e., the target list consists of relatively nearby and face-on disk galaxies). We observed galaxies that had not been extensively studied previously, and used published data when extensive observations were available (e.g., M81, M101). The latter galaxies consisted of Sa-Sm galaxies (whether in the key project sample or not) for which five or more H II regions had been measured. Since our abundance measurements are based on the "empirical" index $R_{23} \equiv$ ([O II] $\lambda\lambda$3726, 3729 + [O III] $\lambda\lambda$4959, 5007)/Hβ (§ 3.5), the published spectra had to include at least these emission lines. In particular we excluded surveys based on measurements of the [O III]/Hβ index alone (e.g., Zaritsky, Elston, & Hill 1990).

Table 1 summarizes the properties of the 39 galaxies in our sample. The NGC number of the galaxy is given in column (1). The distance and absolute magnitude are given in columns (2) and (3) and are adopted from Tully's Nearby Galaxy Catalog (1988). The inclination-corrected maximum circular velocity is presented in column (4) and represents an average of values for one-half of the H I width as presented in the Huchtmeier & Richter catalog (1989). The isophotal radius (the radius at which the surface brightness equals 25.0 mag arcsec^{-2}) was adopted from de Vaucouleurs, de Vaucouleurs, & Corwin (1976, hereafter RC2) and is listed in column (5). The disk scale length as extracted from Boroson (1981), Boroson, Strom, & Strom (1983), Carignan (1985), Elmegreen & Elmegreen (1984, 1985), Kent (1987), Kodaira, Watanabe, & Okamura (1986), Simien & de Vaucouleurs (1986), or Whitmore & Kirshner (1982) is given in column (6). In columns (7) and (8) the galaxy Hubble type and bar type are presented on a numerical scale. The former is referred to as the T-type and is as defined by RC2, while the latter is simply a binary scale in which 0 indicates unbarred and 1 indicates barred. T-type is adopted from RC2. Bar type is adopted from RC2 and our own visual inspections. Finally, in column (9) we have listed the number of H II region observations collected for each galaxy and the references for those data. For those data from the literature, we did not attempt to match multiple observations of the same region; therefore, the number of *distinct* regions observed for each galaxy may be slightly smaller than the number listed in column (7). Due to slight, but possibly significant, differences in quoted positions, we were unable to unambiguously match observations from different studies. Galaxies marked with asterisks were targets of our observations.

The galaxies in Table 1 span a wide range of Hubble types, from Sab to Sm, although our targets are predominantly late types. They also span a wide range of absolute luminosities, from -16.9 (NGC 300) to -21.4 (NGC 1068), although most galaxies lie in the range $-21 < M_B < -19$. Thirty-two of the galaxies are unbarred, and seven are barred. The total sample consists of 39 galaxies, 14 of which we observed, and 577 observed H II regions. As explained above, the last number includes repeat observation of the same region by different investigators. Our observations comprise 159 of the 577 regions. The new observations presented here represent at least 27%, and more likely nearly 35% (since many of the observa-

TABLE 1

THE GALAXY SAMPLE

Galaxy (1)	D (Mpc) (2)	M_B (3)	V_C (km s^{-1}) (4)	ρ_0 (5)	ρ_s (6)	Type (7)	Bar Type (8)	Number of Regions and References (9)
NGC 55	2.3	−20.15	95	11.50	...	9	1.0	6 (1)
NGC 224	0.7	−20.67	276	77.44	15.07	3	0.0	19 (2, 3)
NGC 253	2.5	−20.72	225	9.80	...	5	0.0	8 (1)
NGC 300	1.2	−16.88	120	9.75	3.50	7	0.0	44 (1, 4, 5)
NGC 598	0.7	−18.31	83	28.77	8.24	6	0.0	29 (6, 7, 8)
NGC 628	9.7	−20.32	107	5.36	1.28	5	0.0	7 (6)
NGC 925*	9.4	−19.66	136	5.48	1.24	7	1.0	9 (9)
NGC 1068	14.4	−21.39	252	3.54	...	3	0.0	8 (10)
NGC 1313	3.7	−18.60	156	4.16	1.73	7	1.0	5 (11)
NGC 1365	16.9	−21.26	232	4.46	1.22	3	1.0	11 (4, 11)
NGC 1566	13.4	−20.45	194	3.88	1.89	4	0.0	6 (12)
NGC 2403	4.2	−19.68	150	8.49	2.72	6	0.0	11 (6)
NGC 2541*	10.6	−18.37	124	3.31	...	6	0.0	19 (9)
NGC 2903*	6.3	−19.85	228	6.30	0.97	4	0.0	27 (6, 9)
NGC 2997	13.8	−20.74	240	4.35	...	5	0.0	54 (6, 13)
NGC 3031	1.4	−18.29	268	11.99	2.94	2	0.0	26 (10, 14, 15)
NGC 3184*	8.7	−19.34	329	3.71	...	6	0.0	15 (6, 9)
NGC 3198*	10.8	−19.62	170	4.26	0.92	5	0.0	15 (9)
NGC 3319*	11.5	−18.71	136	3.08	0.98	6	1.0	13 (9)
NGC 3344*	6.1	−18.47	227	3.54	0.83	4	0.0	14 (6, 9)
NGC 3351	8.1	−19.26	205	3.62	...	3	1.0	10 (6, 10)
NGC 3521*	7.2	−19.88	268	4.26	0.81	4	0.0	10 (6, 9)
NGC 3621*	7.1	−19.87	174	4.77	...	7	0.0	7 (9)
NGC 4254	16.8	−20.84	288	2.75	0.64	5	0.0	9 (6,16)
NGC 4258*	6.8	−20.59	234	7.92	2.22	4	0.0	18 (9, 10)
NGC 4303	15.2	−20.71	175	3.08	0.64	4	0.0	22 (16, 17)
NGC 4321	26.6	−21.13	288	3.54	1.06	4	0.0	10 (6, 16)
NGC 4559*	9.7	−20.07	143	5.48	...	6	0.0	20 (9)
NGC 4725*	12.4	−20.65	297	5.36	...	2	0.0	8 (9)
NGC 4736	4.3	−19.37	209	5.48	1.03	2	0.0	9 (6, 10)
NGC 5033*	18.7	−21.03	251	5.36	1.71	5	0.0	8 (9)
NGC 5055	7.2	−20.14	242	5.74	1.71	4	0.0	5 (6)
NGC 5194	7.7	−20.75	250	5.24	1.86	4	0.0	11 (6, 18)
NGC 5236	4.7	−20.31	227	5.87	2.02	5	1.0	10 (1, 19)
NGC 5457	5.4	−20.45	190	14.09	2.11	6	0.0	21 (6, 20, 21)
NGC 6384	26.6	−21.31	275	3.23	1.59	4	0.0	8 (10)
NGC 6946	5.5	−20.78	240	6.59	2.74	6	0.0	7 (6)
NGC 7331*	14.3	−21.10	282	4.77	1.45	4	0.0	8 (9, 10)
NGC 7793	2.8	−17.69	138	4.35	1.46	8	0.0	30 (1, 6)

NOTE.—Asterisks indicate new data obtained as part of this study.

REFERENCES.—(1) Webster & Smith 1983. (2) Dennefeld & Kunth 1981. (3) Blair et al. 1982. (4) Pagel et al. 1979. (5) Deharveng et al. 1988. (6) McCall et al. 1985. (7) Kwitter & Aller 1981. (8) Vílchez et al. 1988. (9) This work. (10) Oey & Kennicutt 1993. (11) Pagel et al. 1980. (12) Hawley & Phillips 1980. (13) Walsh & Roy 1989. (14) Garnett & Shields 1987. (15) Stauffer & Bothun 1984. (16) Shields et al. 1991. (17) Henry et al. 1992. (18) Díaz et al. 1991. (19) Dufour et al. 1980. (20) Smith 1975. (21) Rayo et al. 1982.

tions in the literature are repeat observations, especially true for NGC 598 and NGC 300) of all regions for which R_{23} has been measured for galaxies with five or more observed H II regions.

2.2. *Observing Procedure and Data Reduction*

We selected target H II regions from continuum subtracted Hα CCD images, which we obtained either at the Steward 2.3 m, the KPNO 0.9 m, or the KPNO Burrell Schmidt telescopes. Most of these regions were sufficiently bright to be identified on the television guide camera images. When possible, multiple regions were observed simultaneously by rotating the spectrograph slit. Our aim in target selection was threefold: (1) that the regions be sufficiently bright so that we could obtain a high signal-to-noise (S/N) spectrum, (2) that we obtain good radial coverage of the galactic disk, and (3) that we obtain at least 10 H II regions per galaxy. We nearly accomplished our goals, although there are some galaxies for which we did not obtain high S/N spectra of at least 10 regions or good radial coverage. For example, we did not obtain good radial coverage for NGC 4725 because its bright H II regions are confined to a thin circular ring.

The data were obtained at the Multiple Mirror Telescope (MMT) with the Red Channel Spectrograph using a 600 line mm^{-1} grating blazed at 4800 Å, which we shall refer to as the long-slit mode, or at the Steward Observatory 2.3 m telescope on Kitt Peak, with a standard B&C spectrograph equipped with a cross-disperser and an echellette grating, which we shall refer to as the cross-dispersed mode. We used a 2 × 180 arcsec slit in the long-slit mode. This mode provided coverage from 3500 to 5200 Å with a resolution of ∼9 Å. To obtain the spectral coverage necessary to observe both [O II] and [O III] the dewer was rotated 45° so that the spectra ran diagonally across the CCD. An illustrative fully reduced spectrum obtained via this mode is provided in Figure 1. We used a 4.5 × 16 arcsec slit in the cross-dispersed mode. This mode provided nearly contiguous coverage from 3600 to 9500 Å with a resolution that spans from 2.5 Å at the blue end to 4.8 Å at the red end. An illustrative fully reduced spectrum obtained via this mode is provided in Figure 2. The data were obtained

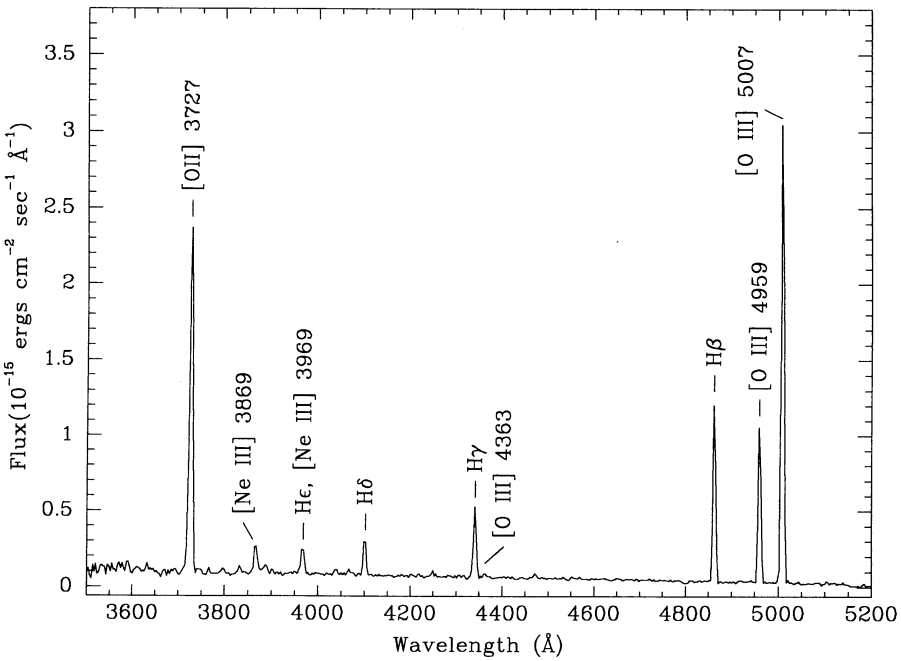

FIG. 1.—Spectrum of region No. 2 in NGC 2541 obtained in the long-slit mode. Emission lines targeted for measurement are labeled.

during observing runs in 1990 January, March, and April (cross-dispersed mode), and during runs in 1990 March and 1991 January and April (long-slit mode).

The observing procedure varied slightly between runs but typically consisted of obtaining bias, flat, and wavelength calibration images at the beginning and end of each night. Several spectrophotometric standards were observed during each night at different air mass. Target exposures varied between 10 and 40 minutes and some exposures were repeated if the spectral S/N was judged insufficient. Fainter targets were generally observed with the MMT, but there is sufficient overlap between the two observing modes for internal consistency checks, which are discussed below. The reduction of long-slit data was done in the standard manner using IRAF.[3] The reduction of the cross-dispersed observations is more complex and warrants further discussion.

[3] IRAF is distributed by the National Optical Astronomical Observatories, which are operated by AURA, Inc., under contract to the NSF.

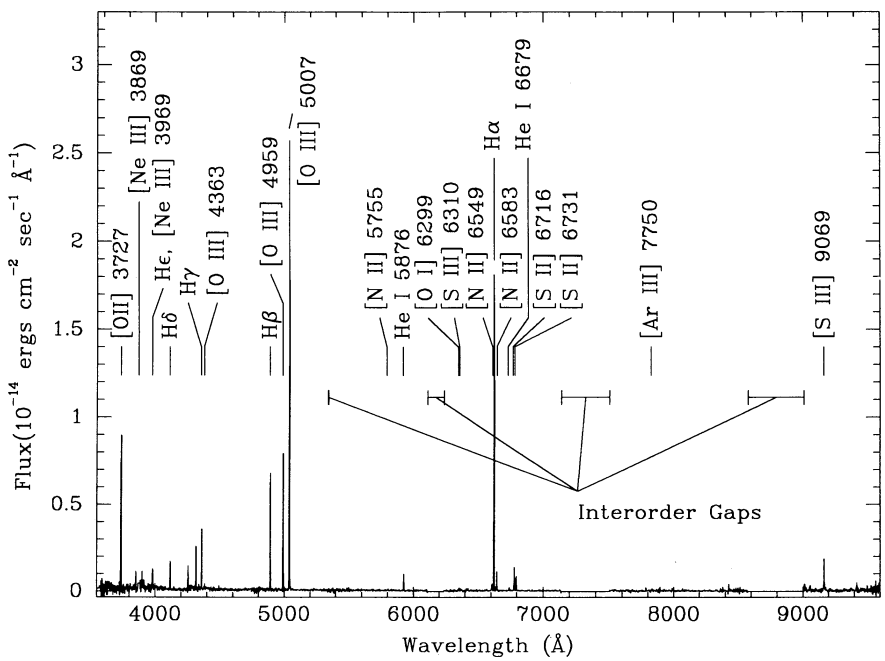

FIG. 2.—Spectrum of region No. 7 in NGC 2541 obtained in the cross-dispersed mode. Emission lines targeted for measurement are labeled.

The cross-dispersed images contain eight orders. Because of the large spectral range, we took both blue and red flats and wavelength calibration lamps. The first four orders were reduced with the blue flat and calibration lamp, the last four with the red ones. The aperture for each order was traced using a standard star observation at low air mass. Calibration lamp exposures were used to rectify and wavelength calibrate each spectrum. All but the last two orders contain about 10 bright calibration lines. The wavelength calibration of the reddest order is extremely poor. Standard star spectra were extracted, corrected using standard extinction laws, and calibrated using existing flux curves for the KPNO IRS standards on the Hayes & Latham (1975) system. The object frames were then flux calibrated. Partial overlap between the first five orders permitted us to make internal checks on both wavelength and flux calibration. Sensitivity curves were constrained near the edges of each order to obtain a continuous spectrum.

Sky subtraction was also more complicated than usual for the cross-dispersed observations. The slit was short (16″) and so the spectra may not include much true sky coverage. The sky subtraction procedure was iterative with the goal of minimizing the scatter in the sky-subtracted spectrum around known sky emission features. Sky apertures were defined interactively on both sides of each H II region spectra. Sky and object spectra were extracted. The sky spectra were then scaled in proportion to the width of the extracted strips and subtracted from the object spectrum. Continua were fitted near the position of each sky line in the sky-subtracted H II spectrum and rms dispersions about the fit were calculated. The sky was rescaled slightly differently and subtracted from the original object spectrum. Again, we evaluated the rms dispersion with respect to the fit in the region around the sky lines. We iterated on this sequence until a minimum in the rms dispersion was found. Before subtracting what was found to be the appropriately scaled sky spectrum, regions of the sky spectrum near the positions of expected emission lines from the H II regions were replaced by continuum fits. This measure assured that the sky subtraction, even if the sky spectrum was contaminated with emission lines, which happened often since the regions are extended, did not artificially diminish the measured emission-line flux. The short slit, and subsequent lack of object-free sky, limits the accuracy of the sky subtraction, especially when the sky is bright and has strong absorption features due to water. For this reason, we present measurements of the [S III] λ9069 line, where we feel the sky subtraction was adequate, but not for the [S III] λ9532 line, where the strong OH sky emission and water absorption were not well subtracted. Although the sky subtraction around [S III] λ9069 appears to have been successful, it is possible that the uncertainties in this line are somewhat larger than our quoted values derived in the manner described below.

One final subtlety of the observing and data reduction process was to minimize the effect of atmospheric refraction. When an object was observed at high air mass, the slit was rotated so that atmospheric refraction would move the object image along the slit. This created spectra that bend even when the frames have been rectified using calibration lamps. The position of the spectra moved by at most 2 pixels from one end of the order to the next, or across the CCD in the long-slit mode. Since the apertures in the cross-dispersed mode are defined using low air-mass standards, corrections must be made. From spectra where either the continuum or several bright emission lines were visible, we calibrated differential refraction versus air mass. That calibration was used to correct spectra of objects that had neither a visible continuum nor multiple bright emission lines.

Once the spectra were extracted and calibrated, the line ratios Hα/Hβ or Hβ/Hγ were measured to determine the effect of dust reddening. The reddening correction was derived from the observed Balmer decrement, using the reddening law as given by Schild (1977), the relative line emissivities given by Osterbrock (1989) for case B recombination, and electron temperatures from the empirical calibration of [O III] flux versus temperature provided by Pagel et al. (1979). An equivalent width of 2 Å for the Balmer line absorption of the underlying stellar continuum was adopted based on the determinations of MRS and OK. The stellar absorption correction amounts to less than 10% for 75% of the regions.

In a few cases the Balmer decrement could not be measured reliably, because the shorter wavelength lines were lost in the noise or one of the lines was distorted by a cosmic-ray event. In such cases we adopted the value of A_V derived for a nearby region, or $A_V = 0$ when there was no observed nearby region. Finally, if the calculated value of A_V was less than 0, we adopted $A_V = 0$. Such corrections were required for only 17% of the regions.

Once the spectra were fully reduced, we combined multiple exposures and measured fluxes of prominent emission lines (see Figs. 1 and 2). Due to the large number of lines and regions observed we automated the line-flux measuring procedure. A polynomial continuum was fitted around the position of each line, excluding the central 18 or 12 Å for the long-slit and cross-dispersed modes respectively. We measured the flux within the line in two separate ways: (1) we integrated under the line from continuum crossing to continuum crossing, and (2) we fitted a Gaussian to the line profile and integrated under the Gaussian from continuum crossing to continuum crossing. The [O II] λ3727 line is slightly resolved into the 3726 and 3729 lines in the cross-dispersed mode. For that "line" only, we fitted two Gaussians and integrated under the sum of the two Gaussians from continuum crossing to continuum crossing. Resulting differences between the two definitions of line flux are slight, typically a few percent in the flux, with each technique appearing to be slightly better on one line profile or another. We averaged the two results to obtain our measured flux. Equivalent widths were evaluated using the polynomial continuum value at the center of the line and the line flux measurement. Line fluxes for lines with signal-to-noise (S/N) ratios less than three (see below for our working definition of S/N) were not retained. Furthermore, a visual check of every line was done to remove pathological cases (e.g., cosmic-ray events, CCD defects, and poor Gaussian fits).

The positions of the observed H II regions, adopted extinctions, and line fluxes of the important diagnostic lines [O II] λ3727, Hβ, [O III] $\lambda\lambda$4959, 5007, [S II] $\lambda\lambda$6716, 6731, and [S III] λ9069 are presented in Table 2. Positions are given as offsets from the nucleus in arcseconds in columns (2) and (3), with north and east positive. Deprojected radii are given in column (4) in terms of isophotal radii. The absorption in the V band is given in column (5) and is highlighted with an asterisk if an adjustment was necessary (see § 2.2 for details). The Hβ flux is given in units of 10^{-16} ergs cm^{-2} s^{-1} in column (6). Fluxes of other emission lines, corrected for reddening and normalized to the flux of Hβ, are listed in columns (7)–(11). The measured Hβ equivalent widths are not presented because they are highly uncertain for many regions. Continuum flux levels are

TABLE 2

EMISSION-LINE FLUXES

NUMBER	OFFSETS N-S	OFFSETS E-W	RADIUS ρ/ρ_0	A_V	Hβ FLUX[a]	EMISSION-LINE FLUXES[b] [O II] λ3727	[O III] $\lambda\lambda$4959, 5007	[S II] λ6716	[S II] λ6731	[S III] λ9032
					NGC 925					
1.....	−1	−205	0.65	1.08	247.3	2.75 ± 0.24	2.85 ± 0.59	0.23 ± 0.04	0.16 ± 0.03	0.14 ± 0.06
2.....	−22	−179	0.60	1.23	191.2	3.60 ± 0.27	3.32 ± 0.67	0.28 ± 0.04	0.21 ± 0.03	0.11 ± 0.05
3.....	17	−236	0.73	1.30	107.1	3.29 ± 0.29	4.07 ± 1.07	0.25 ± 0.05	0.18 ± 0.04	0.18 ± 0.09
4.....	7	−259	0.81	0.49	88.3	2.60 ± 0.31	4.49 ± 1.20	0.33 ± 0.07	0.24 ± 0.06	...
5.....	−3	3	0.02	1.48	34.1	4.02 ± 0.76	2.41 ± 1.30	0.66 ± 0.25	0.39 ± 0.16	...
6.....	−68	−4	0.35	0.93	290.3	1.74 ± 0.17	5.19 ± 1.00	0.19 ± 0.03	0.12 ± 0.02	0.25 ± 0.11
7.....	81	−69	0.42	1.18	122.7	3.93 ± 0.44	1.71 ± 0.57	0.30 ± 0.07	0.20 ± 0.05	0.13 ± 0.06
8.....	−77	60	0.40	0.84	204.3	2.50 ± 0.26	2.06 ± 0.54	0.35 ± 0.07	0.28 ± 0.06	0.23 ± 0.09
9.....	134	29	0.71	0.86	38.7	1.95 ± 0.40	5.89 ± 2.17	0.26 ± 0.08	0.18 ± 0.06	0.21 ± 0.11
					NGC 2541					
1.....	87	11	0.52	0.80	5.7	2.34 ± 0.71	6.78 ± 5.06	0.18 ± 0.12	0.19 ± 0.12	...
2.....	42	−24	0.26	1.25	60.3	3.64 ± 0.77	3.83 ± 1.93	...	...	...
3.....	36	−27	0.27	1.73	33.3	3.74 ± 0.30	4.35 ± 0.86	...	...	...
4.....	30	−27	0.26	0.99	52.9	1.45 ± 0.12	4.46 ± 1.27	...	...	...
5.....	21	−29	0.26	1.49	108.4	3.07 ± 0.20	5.16 ± 1.32	...	...	...
6.....	12	−27	0.24	0.82	41.7	2.25 ± 0.46	4.56 ± 2.46	0.20 ± 0.10	0.12 ± 0.07	0.07 ± 0.09
7.....	12	−26	0.23	0.94	41.1	5.22 ± 0.41	3.42 ± 1.40	...	...	...
8.....	3	34	0.33	0.59	89.3	2.16 ± 0.19	3.73 ± 1.07	...	...	...
9.....	63	29	0.51	1.30	37.7	3.60 ± 0.33	2.00 ± 0.52	...	...	...
10.....	46	12	0.31	2.43	5.1	6.34 ± 0.88	4.17 ± 2.27	...	...	...
11.....	17	71	0.71	1.09	40.3	1.13 ± 0.30	8.97 ± 3.48	0.14 ± 0.05	0.08 ± 0.04	...
12.....	−117	19	0.61	1.39	25.8	4.07 ± 0.37	3.09 ± 1.40	...	...	...
13.....	−67	21	0.35	0.23	3.7	3.87 ± 0.43	2.60 ± 1.24	...	...	...
14.....	−119	−5	0.67	0.23*	22.1	3.32 ± 0.42	2.38 ± 0.91	...	...	...
15.....	−41	−28	0.40	0.54	270.0	1.85 ± 0.10	5.54 ± 0.88	...	...	...
16.....	−27	−47	0.52	0.96	153.4	1.92 ± 0.32	5.53 ± 1.12	0.16 ± 0.03	0.12 ± 0.02	0.18 ± 0.08
17.....	−92	35	0.50	0.79	129.6	2.54 ± 0.25	4.24 ± 0.98	0.20 ± 0.05	0.14 ± 0.04	0.12 ± 0.05
18.....	−49	24	0.20	1.09	46.0	3.58 ± 0.38	2.36 ± 0.83	0.40 ± 0.10	0.26 ± 0.07	...
19.....	−32	88	0.80	0.91	89.3	3.04 ± 0.28	291 ± 0.71	0.36 ± 0.07	0.26 ± 0.05	0.18 ± 0.08
					NGC 2903					
1.....	−75	45	0.45	0.93	53.3	1.48 ± 0.11	0.55 ± 0.15	...	...	...
2.....	−77	41	0.43	0.59	154.2	1.76 ± 0.33	0.70 ± 0.36	0.23 ± 0.08	0.17 ± 0.06	...
3.....	−83	34	0.42	1.92	60.7	1.89 ± 0.32	0.95 ± 0.43	...	...	...
4.....	−65	16	0.28	0.61	251.8	1.75 ± 0.17	0.97 ± 0.23	0.30 ± 0.05	0.20 ± 0.03	0.18 ± 0.07
5.....	−51	25	0.28	1.66	235.4	1.00 ± 0.12	0.31 ± 0.10	0.30 ± 0.05	0.25 ± 0.05	0.19 ± 0.09
6.....	−75	−6	0.23	1.09	276.1	0.44 ± 0.08	0.13 ± 0.06	0.22 ± 0.04	0.17 ± 0.03	0.07 ± 0.03
7.....	36	22	0.12	0.50	205.7	0.30 ± 0.05	0.03 ± 0.02	...	...	...
8.....	25	34	0.17	3.05	51.9	0.54 ± 0.07	0.06 ± 0.02	...	...	...
9.....	61	−4	0.21	1.16	244.1	0.44 ± 0.05	0.05 ± 0.02	...	...	...
10.....	70	−13	0.28	0.92	21.9	1.17 ± 0.14	0.20 ± 0.05	...	...	...
11.....	73	73	0.37	0.59	96.2	2.01 ± 0.19	0.55 ± 0.14	...	...	...
12.....	−118	57	0.64	0.61	33.1	1.61 ± 0.21	0.59 ± 0.19	...	...	...
13.....	−114	59	0.63	1.09	10.8	2.86 ± 0.30	1.59 ± 0.46	...	...	...
14.....	−90	21	0.38	0.60	95.2	2.18 ± 0.27	0.91 ± 0.34	0.57 ± 0.13	0.40 ± 0.09	...
15.....	118	23	0.34	1.75	24.8	1.90 ± 0.15	0.28 ± 0.10	...	...	...
16.....	127	21	0.37	2.94	6.9	4.16 ± 0.35	1.06 ± 0.31	...	...	...
17.....	173	14	0.53	0.40	16.5	1.82 ± 0.18	0.59 ± 0.18	...	...	...
18.....	−95	−65	0.35	2.06	248.2	0.63 ± 0.11	0.12 ± 0.09	0.31 ± 0.08	0.23 ± 0.08	0.08 ± 0.06
19.....	187	172	0.87	0.04	5.9	4.41 ± 0.57	1.99 ± 0.75	...	...	...
20.....	216	172	0.88	0.39	5.6	2.88 ± 0.35	1.90 ± 0.69	...	...	...
					NGC 3184					
1.....	−20	106	0.49	0.15	24.4	1.53 ± 0.21	0.23 ± 0.13	...	...	...
2.....	−20	106	0.49	2.75	10.1	2.08 ± 0.23	0.19 ± 0.06	...	...	...
3.....	68	0	0.31	1.07	43.3	0.79 ± 0.09	0.18 ± 0.08	...	...	...
4.....	73	−8	0.33	0.00*	12.3	1.31 ± 0.19	0.35 ± 0.18	...	...	...
5.....	−97	−20	0.45	0.51	43.0	1.70 ± 0.18	0.43 ± 0.26	...	...	...
6.....	78	−11	0.36	1.07*	16.8	1.27 ± 0.18	0.29 ± 0.15	...	...	...
7.....	−89	−12	0.41	1.31	18.8	1.49 ± 0.28	0.17 ± 0.09	...	...	...
8.....	−41	−59	0.33	0.71	167.6	0.75 ± 0.08	0.14 ± 0.05	...	...	...
9.....	−87	−75	0.53	0.90	101.0	2.10 ± 0.17	0.55 ± 0.12	...	...	...
10.....	−41	−172	0.81	1.34	31.7	3.09 ± 0.20	2.84 ± 0.69	...	...	...

TABLE 2—*Continued*

Number	Offsets N-S	Offsets E-W	Radius ρ/ρ_0	A_V	Hβ Flux[a]	Emission-Line Fluxes[b] [O II] λ3727	[O III] λλ4959, 5007	[S II] λ6716	[S II] λ6731	[S III] λ9032
NGC 3198										
1	−111	−66	0.52	0.58*	10.8	3.44 ± 0.49	2.76 ± 1.06	...	...	...
2	−110	−89	0.56	0.58	169.4	2.78 ± 0.24	2.67 ± 0.77	...	...	...
3	−45	−41	0.25	1.59	155.6	2.51 ± 0.20	1.44 ± 0.52	...	...	...
4	−9	−40	0.34	1.77	62.9	3.16 ± 0.46	2.38 ± 0.78	...	...	...
5	−7	−60	0.54	0.00*	5.8	3.09 ± 0.53	4.31 ± 2.44	...	...	...
6	−30	30	0.48	1.21	111.1	2.57 ± 0.19	2.85 ± 0.64	...	...	...
7	46	71	0.48	1.52	68.8	2.72 ± 0.18	1.32 ± 0.29	...	...	...
8	44	38	0.24	0.00*	5.4	1.78 ± 0.29	0.35 ± 0.22	...	...	...
9	150	83	0.70	2.35	51.3	3.79 ± 0.35	2.39 ± 0.51	...	...	...
10	152	93	0.71	2.08	15.0	3.28 ± 0.31	1.95 ± 0.83	...	...	...
11	−187	−27	1.18	2.78	18.9	7.72 ± 0.73	1.34 ± 0.43	...	...	...
12	113	9	0.76	0.87	27.5	3.55 ± 0.30	4.79 ± 1.40	...	...	...
13	118	16	0.75	1.25	15.9	5.20 ± 0.50	1.35 ± 0.60	...	...	...
14	126	26	0.74	0.00*	7.8	3.96 ± 0.47	5.01 ± 1.88	...	...	...
15	131	36	0.72	0.82	29.5	3.68 ± 0.36	3.09 ± 0.99	...	...	...
NGC 3319										
1	126	70	0.74	2.00*	5.7	5.63 ± 0.57	1.98 ± 0.61	...	...	...
2	115	68	0.68	2.00*	1.3	4.88 ± 0.93	1.64 ± 0.66	...	...	...
3	79	62	0.50	0.00*	68.8	3.68 ± 0.38	3.93 ± 0.89	...	...	...
4	72	47	0.43	2.76	58.1	5.71 ± 0.40	2.55 ± 1.30	...	...	...
5	52	89	0.60	0.24	135.0	1.84 ± 0.17	5.91 ± 1.37	...	...	...
6	−68	21	0.57	0.00*	30.5	1.93 ± 0.38	6.21 ± 2.32	...	...	...
7	−67	−12	0.41	1.31	23.0	4.46 ± 0.27	2.15 ± 0.79	...	...	...
8	−61	−100	0.67	0.67	154.7	2.20 ± 0.26	5.57 ± 1.56	...	...	...
9	−89	−60	0.54	0.81	149.9	2.00 ± 0.25	6.21 ± 2.07	...	...	...
10	−95	−50	0.55	1.38	35.3	5.09 ± 0.36	2.51 ± 0.67	...	...	...
11	−16	−3	0.10	0.55*	2.4	3.37 ± 0.32	1.12 ± 0.53	...	...	...
12	−10	−9	0.07	0.00*	9.8	2.63 ± 0.28	1.23 ± 0.46	...	...	...
13	−12	14	0.17	0.55	5.1	3.55 ± 0.31	1.63 ± 0.57	...	...	...
NGC 3344										
1	25	66	0.35	1.26	74.7	1.96 ± 0.14	0.52 ± 0.16	...	...	...
2	65	50	0.39	1.73	11.3	2.97 ± 0.32	1.02 ± 0.36	...	...	...
3	21	48	0.26	1.09	45.3	2.09 ± 0.16	0.51 ± 0.27	...	...	...
4	74	35	0.39	1.25	39.3	2.73 ± 0.26	1.11 ± 0.27	...	...	...
5	78	26	0.39	1.76	56.0	2.98 ± 0.24	1.10 ± 0.21	...	...	...
6	83	7	0.39	2.31	7.2	3.30 ± 0.36	1.90 ± 0.68	...	...	...
7	158	18	0.75	1.06	105.9	2.27 ± 0.17	5.46 ± 0.68	...	...	...
8	155	9	0.74	1.42	56.2	2.55 ± 0.19	6.46 ± 2.40	...	...	...
9	−41	−90	0.48	0.55	91.0	2.56 ± 0.21	2.04 ± 0.73	...	...	...
NGC 3521										
1	97	13	0.47	0.99	37.2	1.89 ± 0.21	1.46 ± 0.58	...	...	...
2	80	−5	0.34	1.05	34.8	1.19 ± 0.15	0.27 ± 0.13	...	...	...
3	47	−48	0.34	1.64	35.2	2.20 ± 0.21	0.50 ± 0.16	...	...	...
4	43	−48	0.34	1.64*	5.6	2.01 ± 0.29	0.87 ± 0.33	...	...	...
5	−25	−10	0.16	2.13	80.4	1.17 ± 0.25	0.11 ± 0.05	0.23 ± 0.08	0.20 ± 0.07	0.06 ± 0.06
6	−35	40	0.28	1.89	135.5	1.23 ± 0.10	0.24 ± 0.07	...	...	...
7	−97	34	0.40	2.69	72.8	2.57 ± 0.32	0.35 ± 0.21	0.35 ± 0.10	0.28 ± 0.08	0.35 ± 0.25
8	−118	−33	0.66	2.03	84.2	4.09 ± 0.43	4.13 ± 1.33	0.27 ± 0.08	0.18 ± 0.06	0.45 ± 0.27
9	−170	62	0.71	1.63	56.4	3.48 ± 0.55	1.48 ± 0.72	0.35 ± 0.14	0.24 ± 0.10	0.50 ± 0.33
10	31	−48	0.34	1.89*	7.1	1.53 ± 0.31	0.19 ± 0.09	...	...	...
NGC 3621										
1	68	25	0.33	0.68	511.3	2.07 ± 0.16	0.96 ± 0.18	0.33 ± 0.04	0.25 ± 0.03	0.09 ± 0.04
2	95	−10	0.35	0.28	208.9	1.66 ± 0.22	0.79 ± 0.23	0.30 ± 0.06	0.24 ± 0.05	0.06 ± 0.03
3	−15	61	0.31	1.82	174.1	3.16 ± 0.27	1.75 ± 0.44	0.33 ± 0.06	0.22 ± 0.04	0.02 ± 0.01
4	−37	26	0.17	2.90*	72.9	1.79 ± 0.19	0.25 ± 0.13	...	...	...
5	−58	67	0.36	0.95	190.6	3.07 ± 0.25	0.62 ± 0.16	...	...	...
6	−18	29	0.15	2.90	117.3	2.63 ± 0.21	0.60 ± 0.26	...	...	...
7	−68	91	0.48	0.91	62.8	2.37 ± 0.25	2.60 ± 0.90	...	...	...

TABLE 2—*Continued*

Number	Offsets N-S	Offsets E-W	Radius ρ/ρ_0	A_V	Hβ Flux[a]	Emission-Line Fluxes[b] [O II] λ3727	[O III] λλ4959, 5007	[S II] λ6716	[S II] λ6731	[S III] λ9032
NGC 4258										
1	183	−305	1.17	0.00*	46.7	2.72 ± 0.24	1.10 ± 0.33	...	...	...
2	−37	−139	0.78	0.73	79.9	3.11 ± 0.27	2.05 ± 0.54	...	...	...
3	−169	−15	0.62	1.13	78.7	2.41 ± 0.23	0.74 ± 0.27	...	...	...
4	−86	−22	0.37	0.81	1721.3	1.97 ± 0.13	1.45 ± 0.23	0.14 ± 0.02	0.10 ± 0.01	0.38 ± 0.19
5	−67	52	0.19	0.95*	18.0	3.52 ± 0.47	0.21 ± 0.08	...	...	...
6	−37	−1	0.13	0.00*	119.8	1.58 ± 0.16	0.44 ± 0.12	...	...	...
7	−91	18	0.25	0.97	15.5	2.20 ± 0.23	1.68 ± 0.54	...	...	...
8	−393	40	1.18	0.00*	85.9	1.55 ± 0.19	6.65 ± 2.74	...	...	...
9	273	−36	0.80	0.15	69.6	1.57 ± 0.17	1.89 ± 0.33	...	...	...
NGC 4559										
1	−8	11	0.05	0.99	148.1	2.72 ± 0.27	1.04 ± 0.31	0.40 ± 0.11	0.34 ± 0.07	0.21 ± 0.09
2	103	−26	0.37	0.51	285.9	3.05 ± 0.21	2.99 ± 0.59	0.31 ± 0.04	0.22 ± 0.03	...
3	117	−43	0.40	0.37	128.3	2.70 ± 0.27	3.32 ± 0.83	0.26 ± 0.05	0.22 ± 0.04	0.23 ± 0.09
4	−94	−74	0.78	0.37	213.2	2.43 ± 0.24	3.99 ± 0.82	0.15 ± 0.03	0.11 ± 0.02	0.04 ± 0.02
5	−92	135	0.67	2.30	16.2	3.82 ± 0.34	1.77 ± 0.53	...	...	...
6	−113	129	0.62	2.24	25.1	3.31 ± 0.54	1.78 ± 0.51	...	...	...
7	−112	128	0.62	0.77	80.4	3.05 ± 0.60	3.55 ± 2.57	...	...	...
8	−114	124	0.60	1.17	32.7	3.64 ± 0.48	3.71 ± 1.10	...	...	...
9	−153	102	0.56	1.13	75.2	1.75 ± 0.14	4.59 ± 0.83	...	...	...
10	−193	98	0.66	0.80	26.6	4.06 ± 0.35	1.85 ± 0.63	...	...	...
11	−191	95	0.65	1.48	21.0	3.18 ± 0.28	4.63 ± 1.01	...	...	...
12	184	−111	0.65	1.66	25.8	4.42 ± 0.37	2.56 ± 0.76	...	...	...
13	187	−116	0.67	0.80	14.5	5.12 ± 0.44	2.15 ± 0.76	...	...	...
14	170	−81	0.58	0.32	14.3	4.20 ± 0.39	4.19 ± 1.40	...	...	...
15	173	−85	0.59	3.68*	3.9	5.91 ± 0.62	4.72 ± 1.99	...	...	...
16	167	−77	0.57	1.01	4.4	5.37 ± 0.65	3.24 ± 1.40	...	...	...
17	−51	62	0.30	1.06	384.7	2.60 ± 0.23	2.39 ± 0.50	0.30 ± 0.06	0.22 ± 0.04	0.38 ± 0.17
18	−74	41	0.26	0.67	681.6	3.00 ± 0.19	2.22 ± 0.37	0.22 ± 0.03	0.15 ± 0.02	0.34 ± 0.14
19	−17	−14	0.15	0.97	260.4	2.95 ± 0.24	1.12 ± 0.31	0.29 ± 0.06	0.24 ± 0.05	0.30 ± 0.14
20	4	−16	0.09	1.10	279.3	2.70 ± 0.22	0.99 ± 0.26	0.25 ± 0.05	0.19 ± 0.04	0.32 ± 0.14
NGC 4725										
1	42	101	0.40	0.90	93.6	0.90 ± 0.09	0.13 ± 0.05	...	...	...
2	125	50	0.42	0.23	57.9	0.80 ± 0.09	0.14 ± 0.06	...	...	...
3	−95	−120	0.51	1.38	11.8	1.82 ± 0.23	0.36 ± 0.16	...	...	...
4	−127	−66	0.45	0.52	25.3	1.07 ± 0.16	0.10 ± 0.03	...	...	...
5	−120	−47	0.41	1.00*	2.0	3.20 ± 0.74	0.69 ± 0.33	...	...	...
6	124	40	0.41	1.53	26.1	1.75 ± 0.17	0.36 ± 0.15	...	...	...
7	123	20	0.41	1.45	9.4	1.45 ± 0.23	0.13 ± 0.13	...	...	...
8	10	122	0.49	0.90*	12.1	2.61 ± 0.30	0.26 ± 0.07	...	...	...
NGC 5033										
1	−155	144	0.90	2.72	55.5	3.56 ± 0.19	1.21 ± 0.23	...	...	...
2	−215	28	0.68	1.20	35.4	4.04 ± 0.22	1.74 ± 0.36	...	...	...
3	−217	22	0.68	2.63	18.4	6.47 ± 0.51	1.64 ± 0.53	...	...	...
4	−97	52	0.39	2.68	20.5	3.74 ± 0.30	1.18 ± 0.39	...	...	...
5	13	−65	0.39	2.25	30.8	2.60 ± 0.19	1.28 ± 0.29	...	...	...
6	−13	−65	0.41	2.20*	2.4	3.86 ± 0.73	0.68 ± 0.32	...	...	...
7	−33	−66	0.44	2.20*	2.3	3.71 ± 0.40	1.69 ± 0.70	...	...	...
8	28	−14	0.11	1.41*	18.6	0.51 ± 0.06	0.28 ± 0.10	...	...	...
NGC 7731										
1	−5	34	0.35	0.69	48.0	2.17 ± 0.18	1.71 ± 0.41	...	...	...
2	−173	72	0.77	2.50	13.8	3.35 ± 0.44	0.88 ± 0.44	...	...	...

NOTE.—Asterisks indicate A_V as described in the text.
[a] In units of 10^{-16} ergs cm^{-2} s^{-1}.
[b] In units of Hβ flux.

typically quite small, thereby rendering equivalent width measurements untrustworthy, especially for regions observed in the cross-dispersed mode where there is little sky coverage.

2.3. *Uncertainty Estimates*

We have analyzed separately the internal uncertainties in our measurements, arising for example from extraction and sky subtraction errors, and external uncertainties such as those arising from slit positioning, aperture size, and flux calibration. These were evaluated by comparing multiple observations of the same H II regions, either within our data or as compared to published observations. A summary of our comparison is shown in Figure 3, which compares the differences between independent measurements, as described below, as a function of the S/N of the measurement. We measured S/N by dividing the flux in the emission line (the signal) by the rms scatter of the continuum near the emission line with respect to a low-order polynomial fit (the noise) over the width of the line.

We first consider the uncertainty arising from the two techniques used to measure the line flux. We calculated the fractional difference between the result from either method and the mean result for the two methods. These differences have been averaged and binned into equally populated bins as a function of S/N and are plotted as open circles in Figure 3. Regardless of the S/N, the difference between results from the two methods is less than 0.1 (10%).

Next we consider the effect of all reduction uncertainties (extraction, sky subtraction, etc.) by comparing results obtained from multiple exposures of the same target. When comparing multiple exposures from different observing runs, this estimate will also include external sources of error such as slit positioning and flux calibration. In some cases, this comparison will also include the use of different telescopes. Again, we calculate the fractional difference between each observation and the average of the observations. That quantity is averaged, binned, and plotted as solid squares against S/N in Figure 3. We also evaluate internal errors by measuring certain line ratios that have a fixed value, for example, [O III] λ5007/[O III] λ4959, which is fixed at 2.88 (Nussbaumer & Storey 1981). The triangles in Figure 3 represent such measurements (open triangles for [N II] and solid triangles for [O III]). The triangles and the squares lie above the open circles, but are still typically at a level of roughly 0.1.

Finally, the most demanding test comes from a comparison of our results with previously published results for regions in common. These differences will include almost all possible sources of error. However, they will not include such possibilities as the use of the incorrect reddening law, since both studies probably used very similar laws. We have searched the database of MRS, since it is the largest, for regions in common with our sample. Many of the quoted positions for matched regions differ by as much as a few arcseconds and so the differences in line ratios will also reflect variations in flux ratios across the nebulae. We have not binned or averaged these data and present them (again fractional differences from the mean) as crosses in Figure 3. Notice that the differences agree very well with the uncertainties estimated from our own multiple observations. This implies that there are no systematic differences between our study and the MRS study, and that our estimated uncertainties are valid.

As expected, there is a clear trend of decreasing fractional uncertainty with S/N. The dashed line indicates our adopted relationship between S/N and a "1 σ" uncertainty. This calibration allows us to estimate the uncertainty of any emission line from a measurement of S/N. All lines are assigned uncertainties based on this calibration. These uncertainties are propagated through all calculations.

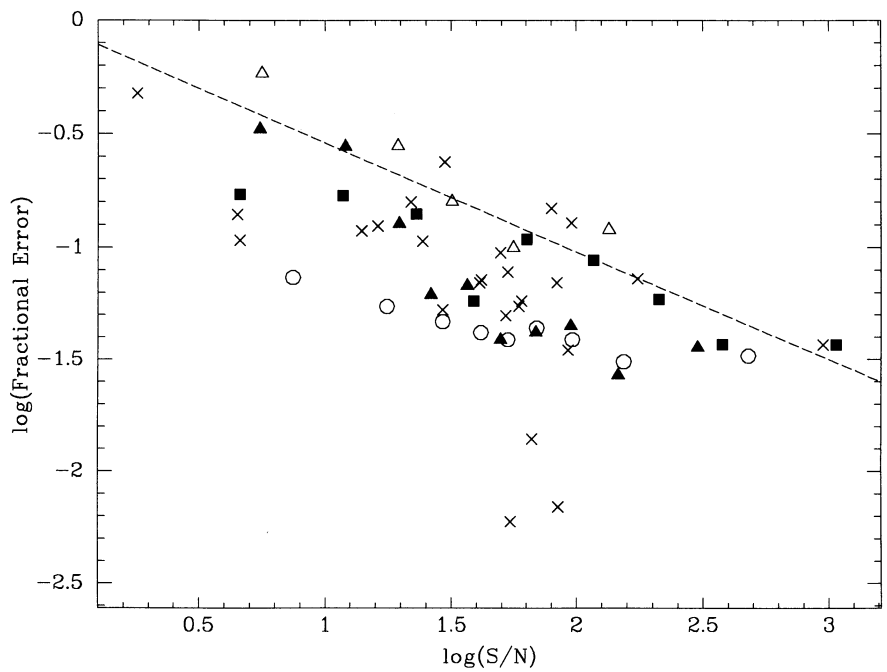

FIG. 3.—Uncertainty Calibration Diagram. Various sources for the estimated uncertainties are plotted (see text for explanation of symbols). The dashed line indicates our adopted calibration of the uncertainty vs. S/N relationship. For example, an emission line with a S/N of 100 would be expected to have an associated uncertainty of about 10%.

3. H II REGION PROPERTIES

The nebular spectra provide information on several physical characteristics of each H II region. The basic parameters that determine the emergent spectrum are the elemental abundances, the gas density, the ionizing spectrum, typically characterized by a temperature T_*, extinction by dust, and the ionization parameter $U \equiv Q/(4\pi R^2 nc)$, where Q is the flux in hydrogen-ionizing photons, R is the radius of the ionized sphere of gas, n is the number density of hydrogen atoms, and c is the speed of light. Below we discuss the behavior of each of these quantities in our sample. We restrict our analysis to data obtained in the cross-dispersed mode, since many of the critical emission lines lie redward of 5200 Å. This restriction reduces the data available, and so we combine the data from various galaxies in order to increase the statistical significance of whatever trends may be apparent. This has the disadvantage that if the variation in properties from galaxy to galaxy are as large or larger than the trend across any particular galaxy, those trends will be obscured.

3.1. *Density*

We have estimated the density in regions observed in the cross-dispersed mode by using [S II] λ6716/[S II] λ6731. The [O II] lines (λλ3726, 3729) are barely resolved and so do not place significant constraints on the density. The [S II] ratios for the 42 regions with available measurements are given in Figure 4. The horizontal line in this figure indicates the low-density limit of 1.42 (Czyzak 1986). Our regions are clearly clustered near this line, but inferences about densities of individual regions cannot be made because of uncertainties in the relevant line fluxes. The weighted mean for the regions is 1.37 ± 0.02. The small deviation from the low-density limit is probably not significant because the line ratio places greater weight on the high-density knots within the emission region (since the ratio can only decrease below 1.42). The values of the ratio are sufficiently near the low-density limit that we infer densities smaller than about 100 cm^{-3}. Hence, collisional effects on line ratios are negligible. This conclusion is in agreement with previous studies of H II regions (e.g., MRS).

3.2. *Ionizing Spectrum*

Several workers have observed a correlation between Hβ equivalent width and oxygen abundance (Shields & Tinsley 1976; Shields & Searle 1978), which is often attributed to changes in the mean temperature T_* of the ionizing stars with metallicity. Subsequent efforts have been made to test for variations in T_*, using the behavior of the ionization of oxygen and sulfur (Sarizin 1976; Shields & Searle 1978; Mathis 1982, 1985). As outlined by Vílchez & Pagel (1988), the temperature of the ionizing stars can be estimated through the use of the parameter η, defined to be $(O^+/O^{++})/(S^{++}/S^+)$. The directly observable quantity, η', is defined by

$$\eta' \equiv \frac{[\text{O II}]\ \lambda\lambda 3726, 3729}{[\text{O III}]\ \lambda\lambda 4959, 5007} \Big/ \frac{[\text{S II}]\ \lambda\lambda 6716, 6731}{[\text{S III}]\ \lambda\lambda 9069, 9532}$$

(Vílchez & Pagel 1988). The relationship between η and η' is

$$\log \eta = \log \eta' + \frac{0.14}{t} + 0.16 ,$$

where t is the electron temperature in units of 10,000 K. As discussed by Vílchez & Pagel, η is virtually reddening and electron temperature independent and is insensitive to the density, but directly related to T_*. Garnett (1989) has studied the sulfur emission of 13 regions in detail and concluded that η is reliable as a relative indicator of the hardness of the ionizing spectrum, but not yet reliable as a quantitative measure of the effective temperature. Detailed modeling is still required to

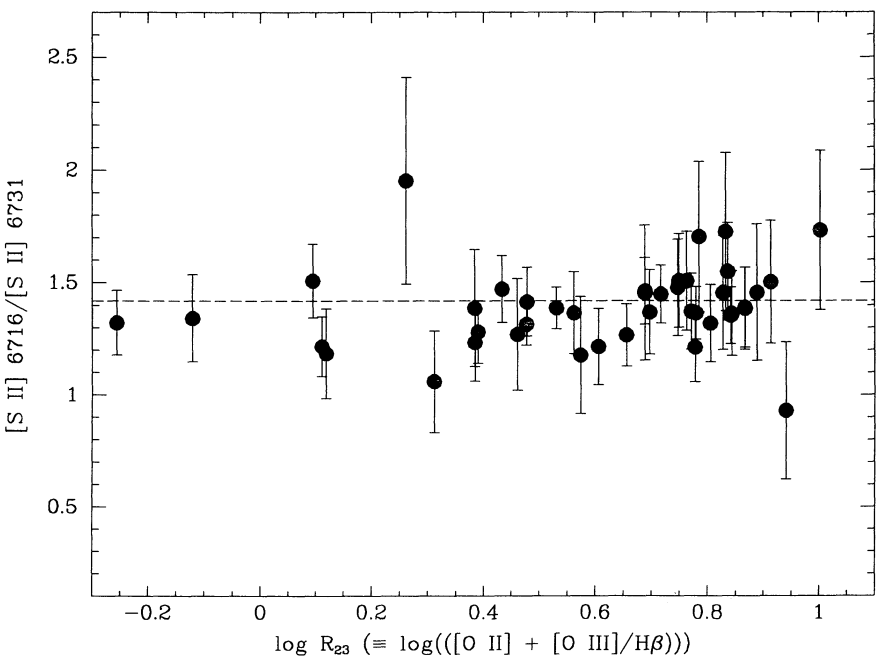

FIG. 4.—The density sensitive ratio [S II] λ6716/[S II] λ6731 is plotted against the oxygen abundance diagnostic R_{23}. The dashed line indicates the low-density limit of that ratio.

derive accurate effective temperatures of the ionizing sources. We will use η to examine the gross properties of T_*.

We can estimate η for the H II regions we observed in cross-dispersed mode by using the measured flux of [S III] λ9069 and the theoretical ratio between the 9532 and 9069 Å lines (2.48; Mendoza & Zeippen 1982). We have plotted the measured values of η versus fractional isophotal radius (radius expressed in units of the isophotal radius of the galaxy) in the left panel of Figure 5. The correlation with radius as found by Vílchez & Pagel is confirmed. Our sample exhibits an anti-correlation between η and fractional isophotal radius at the 97% confidence level as determined using a Spearman rank correlation test. The dashed line, which is the best fit to the data for regions presented by Vílchez & Pagel (we have adopted their lower limit to the outermost point as its actual value), lies noticeably above the bulk of the regions from our sample. Given the uncertainties and the few data in the original work (plotted as open squares without error bars in Fig. 5), the offset may not be significant. Furthermore, for regions with $\rho/\rho_0 < 0.5$, which includes most of the Vílchez & Pagel data, the offset corresponds to only a few thousand degrees (less than 10% of T_*). Some galaxies appear to have definite radial gradients in η (e.g., NGC 4559), others appear to have no gradient (e.g., NGC 2541; as will be shown below NGC 2541 also appears to have an anomalously shallow abundance gradient), and some appear to have systematically different values of η than other galaxies (e.g., NGC 3521 appears to have a systematically larger value of η). We found no significant correlation between the residuals to a best-fit relationship between η and ρ/ρ_0, and R_{23} or Hβ equivalent width (although as mentioned previously the Hβ equivalent width measurements are highly uncertain).

In the right panel of Figure 5 we have plotted η versus log R_{23}. The plot suggests that $\eta = 1$ for $R_{23} < 0.5$, but more data are needed to confirm this trend. Because the temperature sensitive lines ([O III] λ4363 Å) are unavailable at high metallicity, it is critical to understand how the ionizing spectrum behaves as a function of metallicity, since the relation will directly affect the calibration of R_{23} and other empirical abundance tracers.

3.3. *Ionization Parameter*

Since the ionization parameter is related to both the density and the effective temperature of the ionizing source, it may also be estimated using the [S II] and [S III] lines. As given by Díaz et al. (1991), the relationship between the line ratios and the ionization parameter, U, can be expressed as

$$\log U = -1.69 \log ([\text{S II}]/[\text{S III}]) - 2.99$$

over the limited range of values relevant here. We have plotted U for our regions as a function of fractional isophotal radius and log R_{23} (Fig. 6). There appears to be no significant dependence of U on either radius or abundance, although the large scatter would mask any subtle trends. If the lack of a correlation is real, this result would be slightly puzzling in light of the strong relationship between η and radius. These results are in odds with those of Evans & Dopita (1985), who claimed that T_* was nearly constant for all H II regions but that U correlated with abundance. Because the calibration of [S II]/[S III] and U is preliminary and because η might be affected by subtleties of the relative temperatures of the O^+ and O^{++} zones, we are not prepared to extensively discuss these questions. The answer to this question awaits better diagnostics, or detailed modeling, of U, T_*, and η.

3.4. *Redding and Extinction*

If the emergent spectra of H II regions are strongly affected by dust, one might expect their excitation properties to be

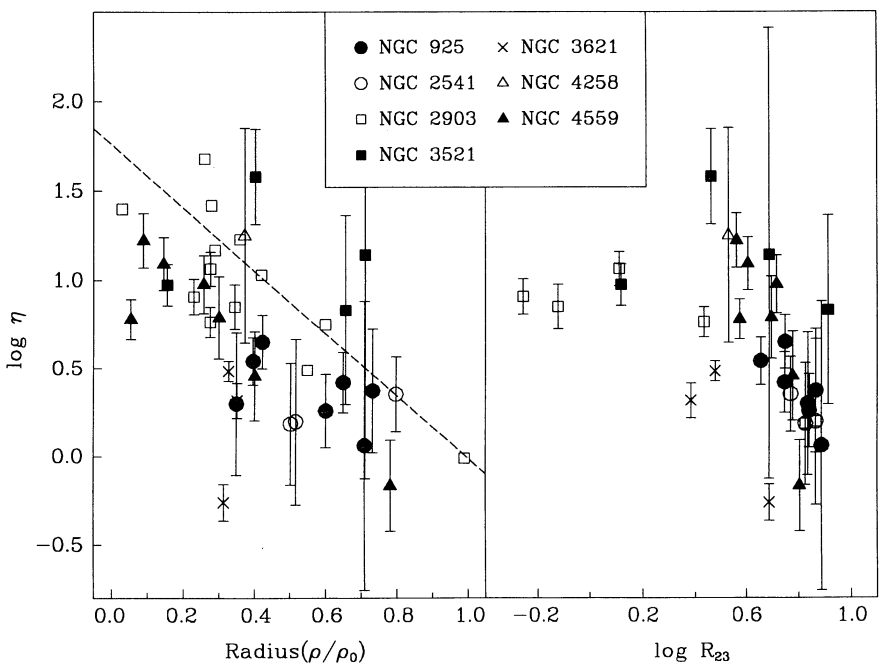

FIG. 5.—Hardness parameter η, which is sensitive to the effective temperature of the ionizing radiation, is plotted vs. fractional isophotal radius (radius in units of the galaxy's isophotal radius) in the left panel and vs. log (R_{23}) {$R_{23} \equiv$ ([O II] $\lambda\lambda$3726, 3729 + [O III] $\lambda\lambda$4959, 5007)/Hβ} in the right panel. Regions from different galaxies coded as given in the legend. Our data are plotted with associated error bars, data from Vílchez & Pagel (1988) are plotted with open squares and no error bars. The dashed line corresponds to a linear fit to the data of Vílchez & Pagel.

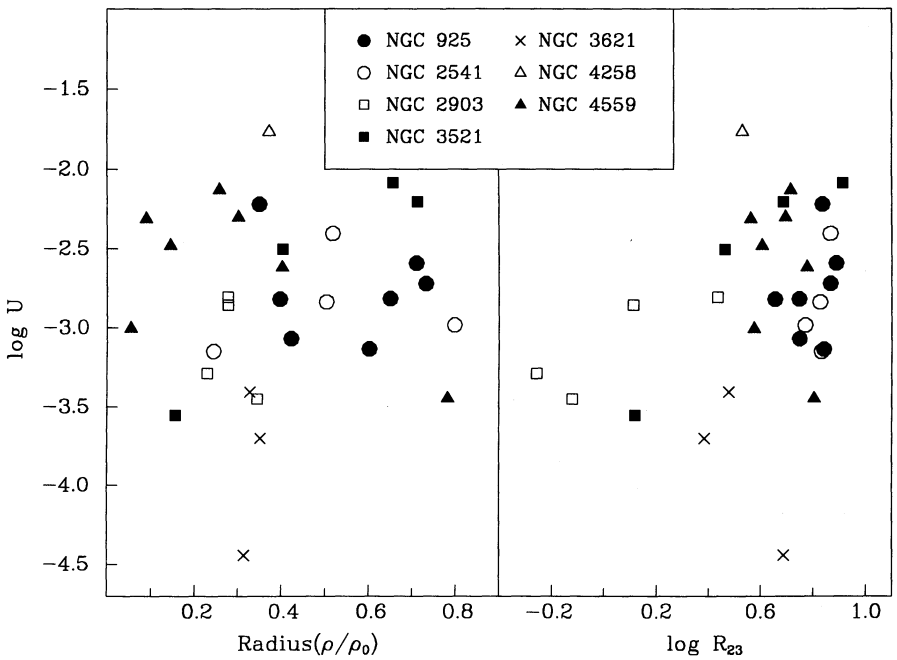

FIG. 6.—Ionization parameter is plotted vs. fractional isophotal radius in the left panel and vs. log (R_{23}) in the right panel. Internal uncertainties, which do not include the uncertainty of the calibration used to obtain U, are of order the scatter between the points and were removed to clarify the diagram. Regions from different galaxies coded as given in legend.

correlated with the observed reddening. We have tested for systematic effects due to dust in two ways. Figures 7*a* and 7*c* show nebular extinction, as derived from the reddening of the Balmer lines, plotted as a function of galactocentric radius for the entire sample (long slit and cross-dispersed data excluding those objects for which adjustments in A_V were necessary) and for regions with Hβ equivalent widths greater than 50 Å, respectively. Although there are large variations in extinction within the sample and systematic variations between some of the galaxies, there is only weak evidence for a radial dependence from Figure 7*c*. Figures 7*b* and 7*d* show extinctions as a function of the abundance parameter R_{23}, as defined in the next section. There is no evidence for a systematic dependence between reddening and abundance.

Our results confirm the conclusions of previous studies, which found at most a weak radial dependence of extinction, less than a few tenths of a magnitude over the entire radial extent of the disk in M51 (van der Hulst et al. 1988), NGC 628 and NGC 6946 (Belley & Roy 1992), and M101 (Scowen, Dufour, & Hester 1992). Our results demonstrate that the large

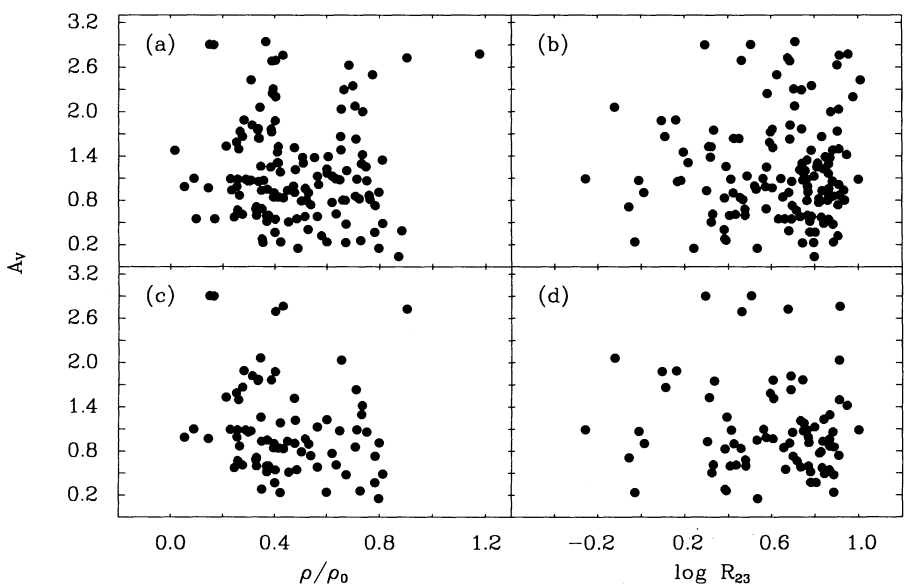

FIG. 7.—Extinction in the V band (A_V) for all regions is plotted against fractional isophotal radius (≡radius/isophotal radius) in the upper left panel (*a*) and against log (R_{23}) in the upper right panel (*b*). Extinction in the V-band (A_V) for regions with Hβ equivalent widths greater than 50 Å is plotted against fractional isophotoal radius in the lower left panel (*c*) and against log (R_{23}) in the lower right panel (*d*).

variations in excitation properties of H II regions within our sample of galaxies cannot be attributed to variations in extinction. They also argue that the large variations in the characteristic Hα luminosities of H II regions along the Hubble sequence are not due to comparable gradients in extinction, but rather reflect differences in the ionizing luminosities of the exciting star clusters (cf. OK). Despite the lack of strong systematic trends in nebular reddening, there is a very large range in extinction, which appears to be mainly local in nature. For example, many of the H II regions in our sample that show the strongest reddening are located within or near prominent dust lanes.

3.5. *Determining the Oxygen Abundance*

Emission lines are the primary source of information regarding chemical abundances within H II regions. Because nebular cooling occurs principally through the escape of photons generated in spontaneous de-excitation of "metal" ions (e.g., oxygen, nitrogen, and sulfur), the strength of the emission lines of these species is an indicator of the electron temperature. From oxygen, the cooling in the nebulae occurs primarily either via fine-structure lines in the far-infrared (52 and 88 μm) when the electron temperature is low or via forbidden lines in the optical (3727, 4959, and 5007 Å) when the electron temperature is high. Since the temperature is high when there is insufficient metal line cooling, high fluxes in the optical lines imply low metallicity. More detailed consideration of the level of ionization of oxygen leads one to consider a line ratio that combines [O II] and [O III] lines in order to sample both the singly and doubly ionized oxygen zones within H II regions.

We convert our measurements of line flux ratios into estimates of the oxygen abundance using existing "empirical" calibrations. Because the temperature sensitive oxygen λ4363 line is so weak, it cannot be observed in the large number of regions required for a study of this kind. The empirical calibrations are based on direct measurements of the electron temperature for low-metallicity regions, and on theoretical models for high-metallicity regions, where they are less reliable. Our oxygen abundance estimates are based on calibrations of the line flux ratio of ([O II] $\lambda\lambda$3726, 3729 + [O III] $\lambda\lambda$4959, 5007)/Hβ. This ratio is referred to in the literature as R_{23} and is believed to be the most useful oxygen diagnostic when the temperature sensitive lines (e.g., [O III] λ4363) are unavailable (Pagel et al. 1979) because it correlates more tightly with oxygen abundance than do other bright-line ratios. The estimated precision of this estimator is roughly 0.2 dex (Pagel, Edmunds, & Smith 1980), although there remain significant systematic uncertainties, especially at the extremes of the abundance range. A comprehensive analysis of the systematics of the R_{23} index for high-abundance regions, based on photoionization models computed for a wide range of physical parameters, can be found in OK.

Various investigators have developed their own calibration of the R_{23} index (e.g., Dopita & Evans 1986; EP; MRS; McGaugh 1991). Many have tried to avoid the pitfalls in a general calibration and tried to fit models either directly to line intensities (e.g., Garnett & Shields 1987) or to multiple diagnostics, such as η and R_{23} (Díaz et al. 1991). The choice of approach depends on the desired accuracy, the number of regions observed, and the quality of the data. We used the R_{23} calibrations of EP, Dopita & Evans (1986), and MRS to estimate the abundance of each region by averaging the derived oxygen abundance from the three calibrations. The difference among the three determinations was adopted as the uncertainty in the derived abundance. In the mean, for the range of interest here the joint calibration for R_{23} is well approximated by

$$12 + \log (\mathrm{O/H}) = 9.265 - 0.33x - 0.202x^2 - 0.207x^3 - 0.333x^4 ,$$

where $x \equiv \log R_{23}$. We find that the dispersion among the abundance estimates from the three calibrations is significantly larger than the internal errors calculated through the propagation of line flux errors. Therefore, our quoted uncertainties in derived abundances, mean abundances, and abundance gradients are calculated using the uncertainty estimates derived from the dispersion between the three calibrations. The advantage of using all three calibrations, instead of choosing whichever one believes to be the most accurate, is that the scatter among the three provides a realistic estimate of the uncertainties in the calibration process.

For data taken from the literature, we have collected the original fully reduced line ratios and applied the same calibration procedure. Nuclear H II regions are excluded from our database because their properties may be quite different than those of regions in the disk (Kennicutt, Keel, & Blaha 1989).

Abundances for all 577 regions, plotted versus fractional isophotal radius, are presented in Figure 8. There is excellent agreement between our data and those from the literature, which confirms our uncertainty estimates, and assures us that the reddening and stellar absorption corrections are plausible.

4. ABUNDANCE PROPERTIES OF SPIRAL GALAXIES

For the remainder of this paper, we will discuss results obtained for the entire sample of galaxies given in Table 1, and focus on galactic properties rather than on properties of individual regions. In this spirit, several preliminary conclusions are immediately apparent from an inspection of Figure 8. There are large differences in both the "mean" abundance and gradients among spiral galaxies. While many galaxies, including such well studied objects as NGC 598 (M33) and NGC 5457 (M101), show strong radial abundance gradients, several of the galaxies in our sample show no gradient whatsoever. Likewise the average abundances range over at least an order of magnitude. As evident from Figure 8, the variations in abundance among regions at the same radius are generally not greater than the uncertainties in the abundance determination. Differences between galaxies are greater than whatever local fluctuations in abundance may be contributing to the scatter. This confirms that variations in abundance and abundance gradients are predominantly global phenomena (i.e., on galactic scales). To quantify these observations we now discuss the global abundance properties of galaxies in detail.

4.1. *Definition of Normalization Radii and Abundances*

Since our principal objective is to compare the global abundance patterns among a large and diverse sample of galaxies, it is important that we adopt consistent criteria for measuring the characteristic abundances and abundance gradients. Unfortunately a wide array of different conventions are used in the literature, many of which are inappropriate for comparing galaxies with different types, luminosities, or structural properties. Here we briefly describe our definitions of normalization radii, mean abundances, and abundance gradients, and some

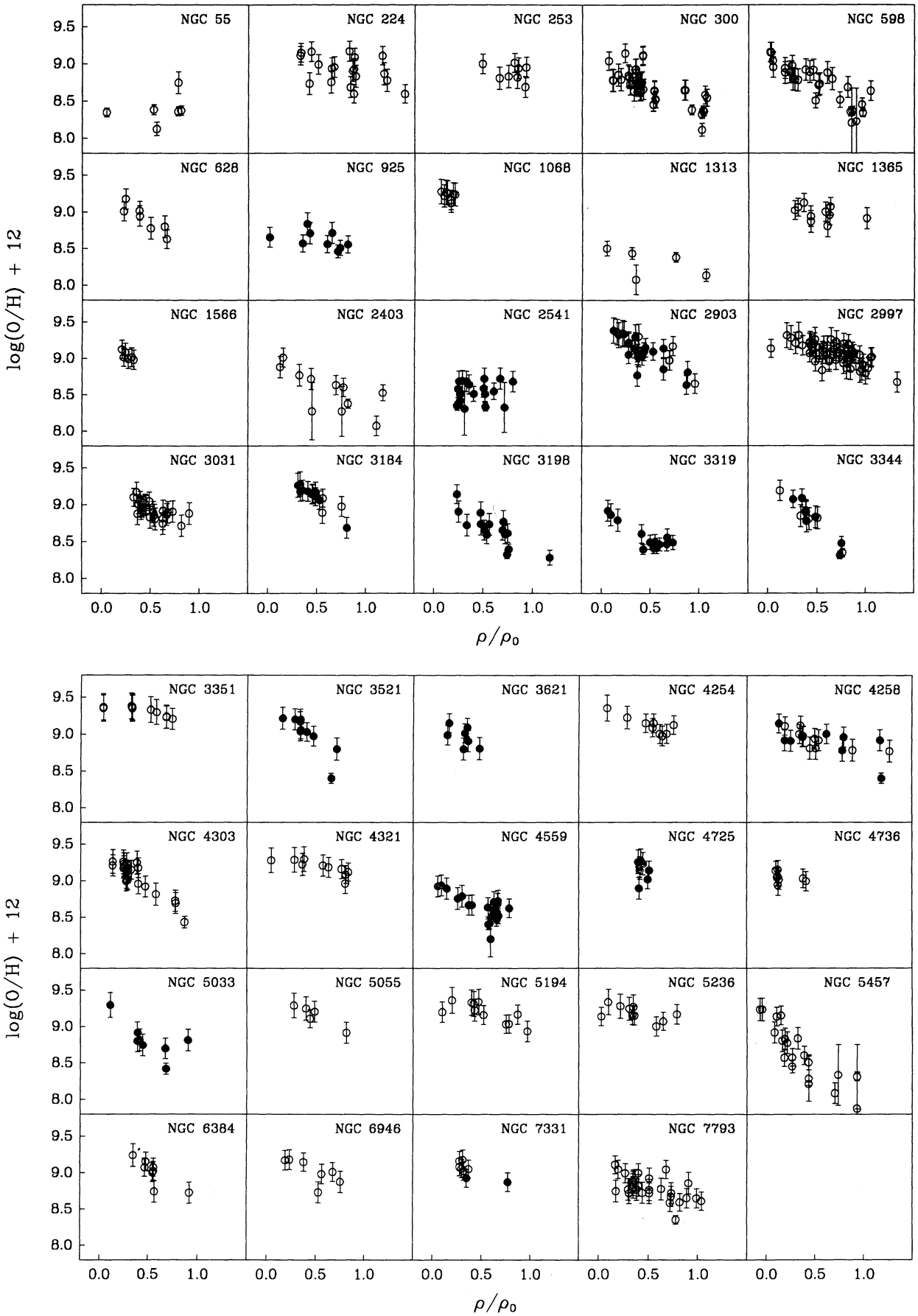

FIG. 8.—Abundances for spiral galaxies with more than five H II regions observed are plotted vs. fractional isophotal radius (≡radius/isophotal radius). Our data are presented with filled circles, while that from the literature is presented with open circles.

of the selection effects that can arise from an inappropriate choice.

We have separately analyzed the disk abundances in terms of three normalization radii: an absolute physical radius (kpc), and two dimensionless radii, normalized to the isophotal radius of the disk (ρ/ρ_0, where ρ_0 is the isophotal radius), and normalized to the disk exponential scale lengths (ρ/ρ_s, where ρ_s is the disk scale length). The choice of radial scaling, or normalization, is critical in a comparison of abundance properties of different galaxies. For example, adopting an absolute radial scale introduces variations among abundance properties that depend directly on disk size. Likewise, measuring mean abundances or abundance gradients in terms of the "effective aperture" or half-luminosity radius will introduce systematic trends with bulge/disk ratio, even for galaxies with identical disk abundances. For most of our discussion we will focus on abundances defined in terms of the fractional isophotal radius, because this radius is less sensitive than most to selection effects of this kind, and because these radii are readily available in the literature (e.g., RC2). Nevertheless, since normalizing to absolute radii or disk scale length may be more physically meaningful for particular applications, we also present our tabulated results in terms of those radii.

The data in Figure 8 demonstrate that there are large differences in the overall disk abundances between different galaxies, regardless of the choice of radius. To quantify these differences it is useful to define a characteristic abundance for each galaxy that is insensitive to the abundance gradients (which will be analyzed independently) and to the radial sampling presented by the observed H II regions. The most frequently used choice for the characteristic abundance in the literature (e.g., VE) is the projected central abundance, which is measured by fitting the radial abundance distribution to an exponential function, and extrapolating to $r = 0$. Unfortunately such projected abundances may often be misleading. They usually require considerable extrapolation from the radii where H II regions are actually observed, they often differ significantly from the actual measured abundance of the nuclear regions, and they are not independent of the abundance gradient (two disks with identical mean abundances but different gradients may differ in projected central abundance by severalfold).

To avoid these problems we compute a weighted linear least-squares fit to the data, and calculate the abundance at 3 kpc, $0.4\rho_0$, and $0.8\rho_s$. These characteristic abundances are nearly the same as the actual measured values at these radii, and they virtually eliminate the need to extrapolate from the observed radii. The characteristic abundances, which we shall henceforth refer to as $\bar{z}$, are listed for each galaxy in our sample in Table 3. They vary from 8.35 for NGC 55 to 9.31 for NGC 3351, when measured at $\rho/\rho_0 = 0.4$. This tenfold range is much

TABLE 3

CHARACTERISTIC ABUNDANCES AND ABUNDANCE GRADIENTS

Galaxy	12 + log (O/H) at $r = 0.4\rho_0$	Gradient (dex/ρ_0)	12 + log (O/H) at $r = 3$ kpc	Gradient (dex/kpc)	12 + log (O/H) at $r = 0.8\rho_s$	Gradient (dex/ρ_s)
NGC 55	8.35 ± 0.07	0.06 ± 0.10	8.35 ± 0.07	0.008 ± 0.013	...	...
NGC 224	9.03 ± 0.09	−0.28 ± 0.10	9.09 ± 0.09	−0.018 ± 0.006	9.10 ± 0.09	−0.05 ± 0.02
NGC 253	8.99 ± 0.31	−0.25 ± 0.35	8.98 ± 0.31	−0.035 ± 0.049	...	...
NGC 300	8.73 ± 0.04	−0.61 ± 0.05	8.44 ± 0.06	−0.179 ± 0.015	8.80 ± 0.04	−0.22 ± 0.02
NGC 598	8.78 ± 0.05	−0.74 ± 0.06	8.70 ± 0.06	−0.127 ± 0.011	8.91 ± 0.05	−0.21 ± 0.02
NGC 628	8.94 ± 0.19	−0.96 ± 0.32	9.13 ± 0.16	−0.063 ± 0.021	9.14 ± 0.16	−0.23 ± 0.08
NGC 925	8.63 ± 0.13	−0.26 ± 0.18	8.68 ± 0.11	−0.017 ± 0.012	8.68 ± 0.11	−0.06 ± 0.04
NGC 1068	9.07 ± 0.53	−0.58 ± 1.24	9.18 ± 0.32	−0.039 ± 0.084	...	...
NGC 1313	8.41 ± 0.09	−0.29 ± 0.11	8.33 ± 0.11	−0.064 ± 0.025	8.43 ± 0.09	−0.12 ± 0.05
NGC 1365	9.01 ± 0.14	−0.19 ± 0.21	9.06 ± 0.12	−0.009 ± 0.010	9.05 ± 0.12	−0.05 ± 0.06
NGC 1566	8.91 ± 0.58	−0.91 ± 1.21	9.10 ± 0.40	−0.060 ± 0.080	8.92 ± 0.57	−0.44 ± 0.59
NGC 2403	8.73 ± 0.10	−0.61 ± 0.12	8.80 ± 0.10	−0.058 ± 0.011	8.82 ± 0.09	−0.19 ± 0.04
NGC 2541	8.48 ± 0.09	0.22 ± 0.15	8.45 ± 0.08	0.021 ± 0.015	...	...
NGC 2903	9.12 ± 0.08	−0.67 ± 0.12	9.22 ± 0.07	−0.058 ± 0.011	9.31 ± 0.07	−0.10 ± 0.02
NGC 2997	9.16 ± 0.06	−0.35 ± 0.08	9.24 ± 0.06	−0.020 ± 0.004	...	...
NGC 3031	9.00 ± 0.13	−0.51 ± 0.19	8.89 ± 0.16	−0.104 ± 0.039	9.10 ± 0.11	−0.12 ± 0.05
NGC 3184	9.18 ± 0.17	−0.92 ± 0.26	9.26 ± 0.16	−0.098 ± 0.028	...	...
NGC 3198	8.78 ± 0.10	−0.87 ± 0.13	8.94 ± 0.09	−0.065 ± 0.010	8.98 ± 0.09	−0.19 ± 0.03
NGC 3319	8.56 ± 0.11	−0.57 ± 0.16	8.63 ± 0.10	−0.056 ± 0.016	8.65 ± 0.10	−0.18 ± 0.05
NGC 3344	8.87 ± 0.10	−1.45 ± 0.14	8.75 ± 0.11	−0.231 ± 0.022	9.17 ± 0.09	−0.34 ± 0.03
NGC 3351	9.31 ± 0.14	−0.23 ± 0.21	9.33 ± 0.13	−0.027 ± 0.025	...	...
NGC 3521	8.97 ± 0.14	−1.71 ± 0.22	9.08 ± 0.13	−0.192 ± 0.025	9.40 ± 0.11	−0.33 ± 0.04
NGC 3621	8.92 ± 0.25	−0.65 ± 0.49	8.98 ± 0.22	−0.066 ± 0.050	...	...
NGC 4254	9.17 ± 0.18	−0.47 ± 0.26	9.26 ± 0.16	−0.035 ± 0.019	9.27 ± 0.16	−0.11 ± 0.06
NGC 4258	8.97 ± 0.06	−0.49 ± 0.08	9.07 ± 0.06	−0.031 ± 0.005	9.06 ± 0.06	−0.14 ± 0.02
NGC 4303	9.01 ± 0.08	−1.06 ± 0.12	9.20 ± 0.06	−0.078 ± 0.009	9.25 ± 0.06	−0.22 ± 0.03
NGC 4321	9.23 ± 0.14	−0.32 ± 0.18	9.32 ± 0.12	−0.012 ± 0.007	9.28 ± 0.13	−0.10 ± 0.06
NGC 4559	8.66 ± 0.10	−0.63 ± 0.14	8.79 ± 0.09	−0.041 ± 0.009	...	...
NGC 4725	9.15 ± 0.73	−0.43 ± 1.22	9.26 ± 0.57	−0.022 ± 0.063	...	...
NGC 4736	9.01 ± 0.17	−0.17 ± 0.37	9.00 ± 0.18	−0.025 ± 0.055	9.05 ± 0.10	−0.03 ± 0.07
NGC 5033	8.84 ± 0.16	−0.86 ± 0.22	9.09 ± 0.13	−0.030 ± 0.008	8.96 ± 0.14	−0.28 ± 0.07
NGC 5055	9.21 ± 0.25	−0.69 ± 0.37	9.31 ± 0.22	−0.058 ± 0.031	9.32 ± 0.22	−0.21 ± 0.11
NGC 5194	9.23 ± 0.12	−0.37 ± 0.17	9.28 ± 0.11	−0.032 ± 0.014	9.27 ± 0.12	−0.13 ± 0.06
NGC 5236	9.16 ± 0.12	−0.19 ± 0.19	9.17 ± 0.11	−0.024 ± 0.024	9.19 ± 0.10	−0.07 ± 0.07
NGC 5457	8.52 ± 0.06	−0.93 ± 0.08	8.76 ± 0.05	−0.042 ± 0.004	8.78 ± 0.05	−0.14 ± 0.01
NGC 6384	9.15 ± 0.23	−0.90 ± 0.34	9.40 ± 0.20	−0.036 ± 0.013	9.16 ± 0.23	−0.44 ± 0.17
NGC 6946	9.06 ± 0.17	−0.55 ± 0.26	9.13 ± 0.15	−0.052 ± 0.025	9.10 ± 0.16	−0.23 ± 0.11
NGC 7331	9.03 ± 0.19	−0.48 ± 0.33	9.15 ± 0.14	−0.024 ± 0.017	9.10 ± 0.15	−0.15 ± 0.10
NGC 7793	8.82 ± 0.07	−0.57 ± 0.09	8.57 ± 0.10	−0.160 ± 0.027	8.90 ± 0.06	−0.19 ± 0.03

larger than the typical uncertainty in the measurements (~0.1 dex). Although the absolute abundances are sensitive to the choice of normalization radius (Table 3), the ranking of galaxies by $\bar{z}$ remains fairly consistent for the three definitions. This is not the case for the abundance gradients, as discussed next.

To quantify radial abundance variations, we use the same computed weighted linear least-square fits to the measurements of log (O/H) versus radius as used for $\bar{z}$. We discuss whether single exponential fits are appropriate in § 4.3.1. Also as above, we adopt three normalizations of radius (units dex/kpc, dex/ρ_0, and dex/ρ_s), but restrict most of our discussion to gradients normalized to the isophotal radius (dex/ρ_0). In these units the measured slopes, which we shall henceforth refer to as G, range from −1.71 for NGC 3521 to +0.22 for NGC 2541. Again, the observed variations are much larger than those that can be attributed to observational uncertainties. In this case the choice of radial scaling is important. For example, NGC 7793 has a steep gradient in units of dex/kpc relative to the other galaxies, but only a moderate gradient in units of dex/ρ_0.

Finally, we address quantitatively the relative uncertainties in $\bar{z}$ and G as a function of sample size. How many H II regions must be measured to reliably determine these quantities? We analyzed data from galaxies that contain at least 20 observed regions. From those data, we randomly selected subsamples of regions, evaluated $\bar{z}$ and G, and then compared those values to those derived from the complete samples. The dispersion in $\bar{z}$ and G, derived from many random drawings, is shown as a function of sample size in Figure 9. The improvement in the determinations rapidly decreases for subsamples containing at least five regions, which suggests that five regions (well spaced in radius) are the minimum number on which one should base determinations of $\bar{z}$ and G.

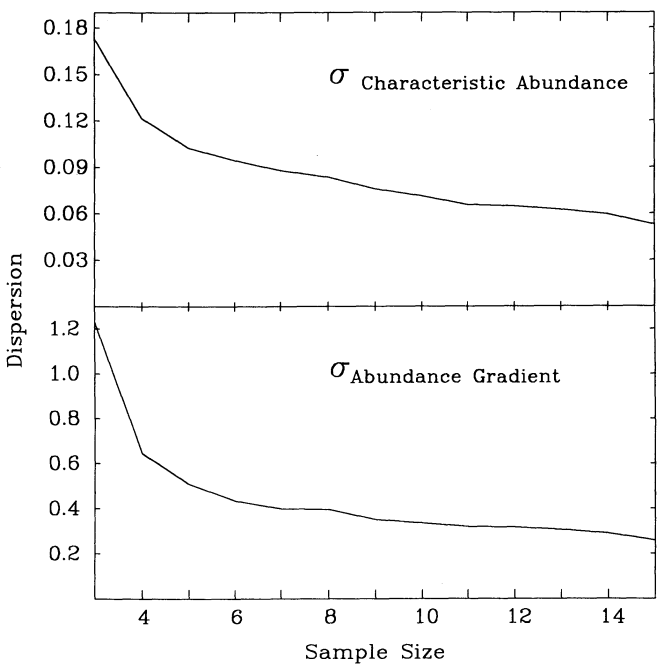

FIG. 9.—Estimated uncertainties associated with measurements of the characteristic abundance and abundance gradient in a galaxy are plotted as a function of the number of H II regions observed in the galaxy. The characteristic abundance is that derived at 0.4ρ_0. The abundance gradient is in units of dex/ρ_0.

4.2. *Discussion*

4.2.1. *Characteristic Abundance and Galaxy Properties*

The significant variation in $\bar{z}$ and G among galaxies in our sample must have an underlying physical cause. The abundances of H II regions in each galaxy exhibit far less scatter (apart from the radial gradients) than among different galaxies, and hence the differences in abundance properties must be the result of *global* phenomena, not of local effects unrelated to properties of the host galaxy. One possibility is that the abundance properties of a galaxy are directly driven by the macroscopic properties of the galaxy. The second possibility is that although abundance is driven by local properties such as surface density or gas fraction, those quantities are largely driven in turn by the macroscopic properties of the galaxy. In general, most properties of galaxies depend on either Hubble type (e.g., gas fraction and the history of star formation), or mass (e.g., luminosity). Therefore, we first examine whether $\bar{z}$ and G correlate with either of these quantities.

We begin by discussing possible dependences between $\bar{z}$ and galaxy properties. In Figure 10 we have plotted $\bar{z}$ (defined in terms of ρ/ρ_0) versus absolute blue magnitude (M_B), inclination-corrected circular velocity (V_C), and Hubble type (T). The characteristic abundance $\bar{z}$ correlates strongly with all three properties, regardless of which scaling of $\bar{z}$ is chosen (not shown). The correlation between $\bar{z}$ and V_C appears slightly tighter than that with M_B, although both are highly significant. In Table 4 we list values of the Spearman rank correlation coefficients for various combinations of observables, along with the probability that such correlations would occur randomly. We prefer V_C to M_B as a mass indicator because the rotation velocity is a better measure of the disk mass, especially for a galaxy sample with a variety of Hubble types and hence a variety of mass-to-light ratios. It also has the advantage of being a distance independent variable. The third panel in Figure 10 clearly demonstrates that a strong T-$\bar{z}$ relationship exists.

Although a first inspection of Figure 10 suggests that abundance is independently correlated with Hubble type and mass, this is not necessarily the case, because galaxy type and mass

TABLE 4

CORRELATION COEFFICIENTS

Variables	Correlation Coefficient	Probability
M_B vs. O/H(ρ_0)	−0.550	0.000
V_C vs. O/H(ρ_0)	0.724	<0.0001
T vs. O/H(ρ_0)	−0.643	<0.0001
M_B vs. O/H(physical)	−0.697	<0.0001
V_C vs. O/H(physical)	0.712	<0.0001
T vs. O/H(physical)	−0.634	<0.0001
M_B vs O/H(ρ_s)	−0.448	0.013
V_C vs. O/H(ρ_s)	0.670	0.0001
T vs. O/H(ρ_s)	−0.646	0.0001
M_B vs. G[O/H(ρ_0)]	0.079	0.63
V_C vs. G[O/H(ρ_0)]	0.056	0.73
T vs. G[O/H(ρ_0)]	−0.019	0.91
M_B vs. G[O/H(physical)]	−0.441	0.0043
V_C vs. G[O/H(physical)]	0.289	0.071
T vs. G[O/H(physical)]	−0.242	0.13
M_B vs. G[O/H(ρ_s)]	0.045	0.81
V_C vs. G[O/H(ρ_s)]	0.147	0.44
T vs. G[O/H(ρ_s)]	−0.139	0.46

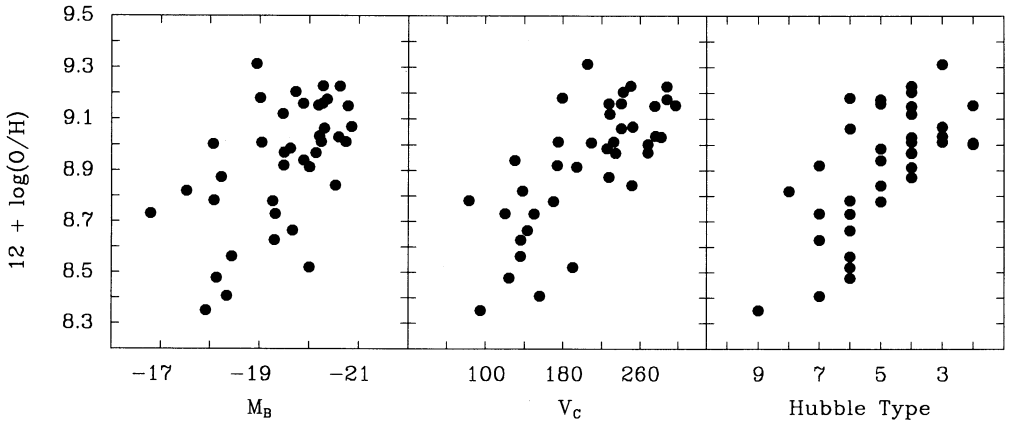

FIG. 10.—Characteristic abundance, defined as the abundance at $r = 0.4\rho_0$, where ρ_0 is the isophotoal radius, is plotted vs. absolute blue magnitude, inclination corrected maximum circular velocity, and Hubble type expressed in units of T-type (smaller T-types are earlier type galaxies).

are correlated with each other among spirals. This is shown explicitly in Figure 11, which shows the T versus V_C relation for the spirals in our sample. As a result it is not obvious to what extent mass or Hubble type may be driving $\bar{z}$. One way to separate the respective dependences is to compute a best fit to the relationship between $\bar{z}$ and V_C (or T), and test whether the residuals from this fit are correlated with T (or V_C). Such residual plots are shown in Figure 12. The absence of any significant correlation in the residuals argues that most of the systematic variation in characteristic abundances is due to a single parameter that is correlated with mass and Hubble type, that is, we cannot detect any independent dependence on type apart from mass. Our conclusion differs from that of OK, who found evidence that early-type spirals (Sa-Sb) were slightly more metal-rich than Sbc-Sc galaxies of the same luminosity. The difference between these results may be attributable to the different samples employed. OK compared all of the early-type galaxies in their sample with the MRS sample of late-type spirals, regardless of the number of H II regions measured. Our sample of late-type spirals is more complete, but by restricting our sample to galaxies with at least five measured H II regions, we have excluded a number of metal-rich early-type spirals in the OK sample. What is clear from both studies is that a single parameter tied to both type and mass is the primary driver of $\bar{z}$ in disks, and that any correlation with type independent of mass is of secondary importance. More complete observations of galaxies spanning the full range of type and luminosity will be needed to determine whether mass or type individually is the predominant driver of $\bar{z}$.

The rms scatter about the linear fit to the relationship between V_C and $\bar{z}$ is 0.17, which corresponds to a factor of about 1.5 in abundance at any value of V_C. In addition to the measurement uncertainties quoted in Table 3, the scatter in $\bar{z}$ must include uncertainties resulting from the radial scaling

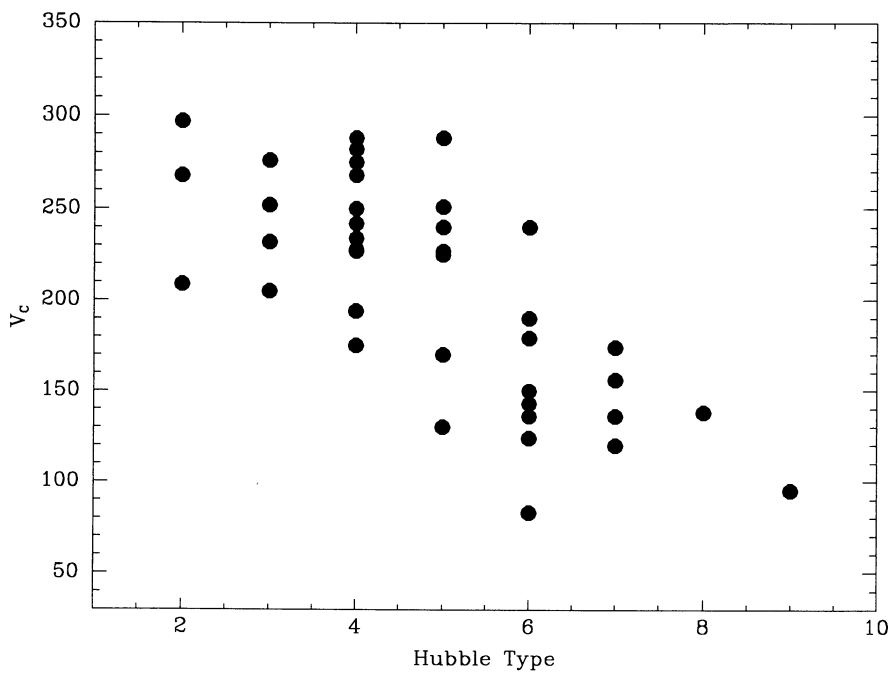

FIG. 11.—The correlation between rotational velocity and T is shown for galaxies in our sample

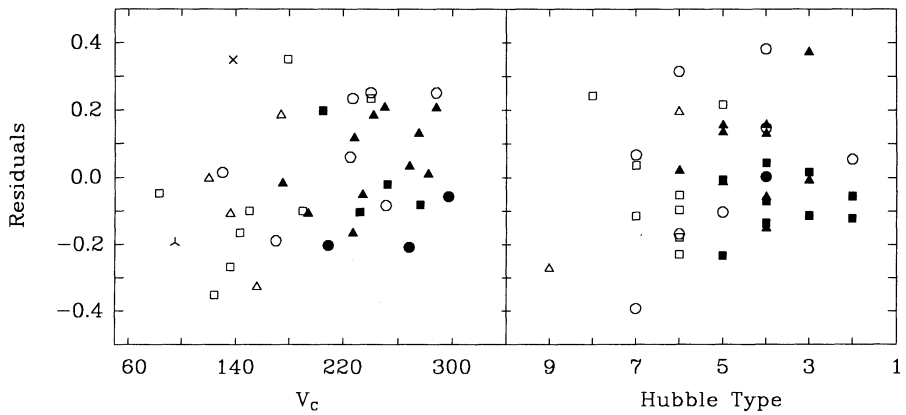

FIG. 12.—The residuals to correlations shown in Fig. 10 are plotted for V_C and T. In the right panel we present the residuals to the $\bar{z}$-T relationship plotted vs. V_C. In the left panel we present the residuals to the $\bar{z}$-V_C relationship plotted vs. T. The left panel is coded by Hubble type (2–9; *filled circle, filled square, filled triangle, open circle, open square, open triangle, cross, triangular cross*).The right panel is coded by V_C ($V_C < 100$ km s^{-1} *open triangle*, $100 < V_C < 150$ km s^{-1} *open square*, $150 < V_C < 200$ km s^{-1} *open circle*, $200 < V_C < 250$ km s^{-1} *filled triangle*, and $V_C > 250$ km s^{-1} *filled square*).

(i.e., inexact knowledge of ρ_0) and from inclination corrections to V_C, which are significant because face-on galaxies were preferentially observed. For these reasons, the intrinsic relationship between $\bar{z}$ and V_C is probably tighter than observed; however, given the significant uncertainties, there is yet no motivation for including a second parameter.

Our analysis so far has dealt entirely with correlations to global properties, and it is likely that variations in local properties, such as disk surface density (EP and VE) are responsible for some of the scatter in Figures 10 and 12. An analysis of the local dependence of disk abundances is beyond the scope of this paper. A follow-up study, based on spatially resolved measurements of the gas, starlight, and mass distributions in the disk is in progress; in the meantime we refer the reader to VE for an up-to-date discussion of this subject.

We have augmented our database of characteristic abundances with published data for less luminous spirals, irregulars, ellipticals, and dwarf spheroidal galaxies, in order to examine the luminosity-metallicity relationship over a larger range of luminosity, galaxy type, and metallicity. We have adopted abundances and magnitudes for ellipticals from the compilations by Brodie & Huchra (1991) and Bender et al. (1993), for irregulars from Skillman, Kennicutt, & Hodge (1989) and references therein, and for dwarf spheroidals from Aaronson (1986). For the Bender et al. sample of ellipticals we converted Mg_2 to [Fe/H] using the calibration from Terlevich et al. (1981) plus a slight offset so that the estimates of [Fe/H] agreed in the mean with those of Brodie & Huchra. For the dSph we converted the published values of M_V to M_B by using $B-V = 0.65$ (as appropriate for dE's; Hodge 1971). The resulting abundance versus luminosity relations are shown in Figure 13. We have plotted the elliptical and spheroidal galaxies separately from the spirals and irregulars, because the interpretation of both the abundances and luminosities differ between the data sets. For the irregulars, $\bar{z}$ was measured from H II regions, and should be directly comparable to $\bar{z}$ for the spirals. Although the definition of mean abundance is different for the irregulars, those galaxies have small (if any) abundance gradients (Pagel et al. 1978), so the quoted values of $\bar{z}$ should be close to the true average. The abundances shown for the E and dSph galaxies (upper panel of Fig. 13) are quite different, since they refer to mean *stellar* abundances (and [Fe/H] rather than [O/H]) in evolved populations, rather than present-day gas phase abundances. Because the variation in mass-to-light ratio among the galaxies is much smaller than the range in luminosity shown in Figure 13, the $\bar{z}$ versus M_B relations imply the existence of similar correlations between abundance and galaxy mass.

The bottom panel of Figure 13 shows the abundance-luminosity relation for gas-rich galaxies (spirals and irregulars). Garnett & Shields (1987) demonstrated that a luminosity-metallicity relationship exists over a wide range of magnitudes between spirals and irregulars, although from their data such a relationship does not appear to exist among the subsample of giant spirals with $\log(M/M_\odot) \gtrsim 11$. Our results indicate that it does. Furthermore, Figure 13 shows that the individual $\bar{z}$ versus M_B relationships among spirals and irregulars merge to form a correlation that spans over 10 magnitudes in M_B, and over a factor of over 100 in $\bar{z}$. This rather impressive correlation suggests that the relationship between $\bar{z}$ and V_C for giant spirals is a continuation of the luminosity-metallicity relationship among irregulars.

A similar relationship is seen for the elliptical and dSph galaxies (Faber 1973; Brodie & Huchra 1992; Bender et al. 1993), and it spans 13 magnitudes and a factor of over 200 in abundance, as illustrated by the upper panel in Figure 13. In this figure we also show the linear fit to the luminosity-abundance relationship for ellipticals as determined by Brodie & Huchra (1991), using those ellipticals for which the uncertainty in [Fe/H] is less than 0.6 dex. This linear fit matches exactly onto the dSph galaxies. The same line is plotted in the lower panel for reference. An offset between the data in the lower panel and the line could result from [O/Fe] $\neq 0$, and the differences between mean stellar versus current gaseous abundances. The relationship for the spirals and irregulars is also slightly steeper than that for the ellipticals and dSph's. As the gas in the irregulars is converted to stars and as the stars age, the irregulars will fade and [O/H] will increase. Both of these effects will, with time, make the spiral and irregular correlation more similar to the elliptical correlation (possibly with a vertical offset related to [O/Fe] $\neq 0$).

What is the physical cause of the luminosity-metallicity or mass-metallicity relationship? For small galaxies, supernovae-wind-driven gas outflow is a plausible mechanism for limiting the abundance, but why should the giant galaxies be part of the same relationship? It might seem unlikely that sufficient

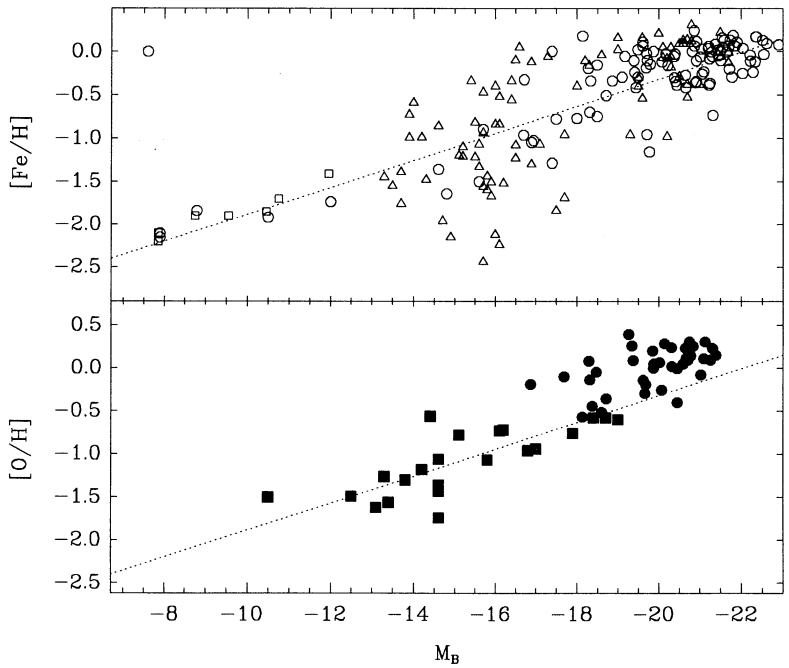

FIG. 13.—Luminosity and metallicity data for Local Group dE's (*open squares*), irregulars (*filled squares*), giant spiral galaxies (*filled circles*), and ellipticals (*open circles*: Bender et al. 1983; *open triangles*: Brodie & Huchra 1991). References and details regarding any necessary conversion are given in text. The abundances for the spiral galaxies are those measured at $r = 0.4\rho_0$. The line in the upper panel is the fit provided by Brodie & Huchra (1991) for E galaxies in their sample with $\sigma_{[Fe/H]} < 0.6$. Their sample did not include the dSph galaxies in the upper panel. The same line is plotted in the lower panel for reference.

material escapes from a giant galaxy to account for the correlation. Nevertheless, there is evidence for large gaseous outflows from starbursting galaxies (Heckman, Armus, & Miley 1990), and Franx & Illingworth (1990) have noted that within ellipticals the abundance correlates with the local escape speed. On the other hand, it appears plausible that stochastic collective effects in giant galaxies, such as starburst and accretion events, would create significant scatter among the abundances of giant galaxies. For example, M82 which is undergoing a starburst phase, and possibly producing stars with a top-heavy IMF (Rieke et al. 1980), might end up more oxygen-rich than a similar galaxy that has not undergone this starburst phase. Although the effect on $\bar{z}$ of such a process depends on the resulting gas fraction, naively one would expect galaxy properties to exhibit significant scatter. In massive galaxies, such as M82, which are already relatively metal rich, it is more difficult to significantly alter $\bar{z}$, than it would be in a low-mass, low-metallicity galaxy. Nevertheless, the scatter about the $\bar{z}$-luminosity relationship does not appear to increase with decreasing luminosity. Our observations suggest that such variations in abundance cannot be greater than about a factor of 1.5 for the range of luminosities or masses of galaxies in our sample. Among ellipticals, Bender (1992) has noted that abundance anomalies correlate with kinematic distortions indicative of mergers (e.g., counterrotating disks); nevertheless, the Mg_2 abundance-velocity dispersion correlation is very tight (Bender 1992). Mould (1984) discussed how early mergers of gas-rich galaxies might not affect the mass-metallicity relationship, but late mergers must affect it. Last, the hypothesis that the modulation of abundances on a galactic scale, at least for giant galaxies, occurs since the earliest times is supported by the correlation between the mean abundance of the globular cluster system and the luminosity of the parent galaxy (Brodie & Huchra 1991). The tight mass-metallicity correlations and the globular cluster metallicity-parent mass correlation indicate that the abundance properties are imprinted early in the evolution of a galaxy.

The correlation between $\bar{z}$ and T among spirals is somewhat more difficult to explain than that with mass, since T itself is not a physical parameter. If mass is not the principal abundance driver, a physical parameter or evolutionary process that correlates with T, such as gas fraction or merger frequency, must be. Unfortunately, we can only estimate the gas fraction (gas mass/total mass) for a small subsample of the galaxies. If gas fraction drives the T-$\bar{z}$ correlation, then one would expect that the correlation between it and $\bar{z}$ would be tighter than that between T and $\bar{z}$. A literature search revealed published CO and H I data for 14 of the 39 galaxies in our sample. We combined these data with optical photometry and mean mass/light ratios to estimate the gas mass fractions of the disks (denoted here as μ_g), following the methods described in Kennicutt & Martin (1993). In this case the data refer to the mass fraction within the star-forming disk ($\rho < \rho_0$), that is, over the same region where the abundances are measured. The resulting $\bar{z}$ versus μ_g relation is shown in the left panel of Figure 14. For our admittedly small subsample that does not include objects with large μ, where the correlation is likely to be most noticeable (Garnett & Shields 1987), we do not find a significant correlation between $\bar{z}$ and gas fraction. We can enlarge the comparison by plotting $\bar{z}$ as a function of relative H I content alone, using $M(\text{H I})/L_B$ values from Tully (1988). In this case there is evidence of a weak correlation, as shown in the right panel of Figure 14. It is interesting that $\bar{z}$ should correlate better with total H I content, since the H I traces only part of the gas, and much of the H I mass is contributed by material well outside the star-forming disk. However, even the correlation with H I content may largely be an artifact of the luminosity-abundance relation; a residual test similar to that

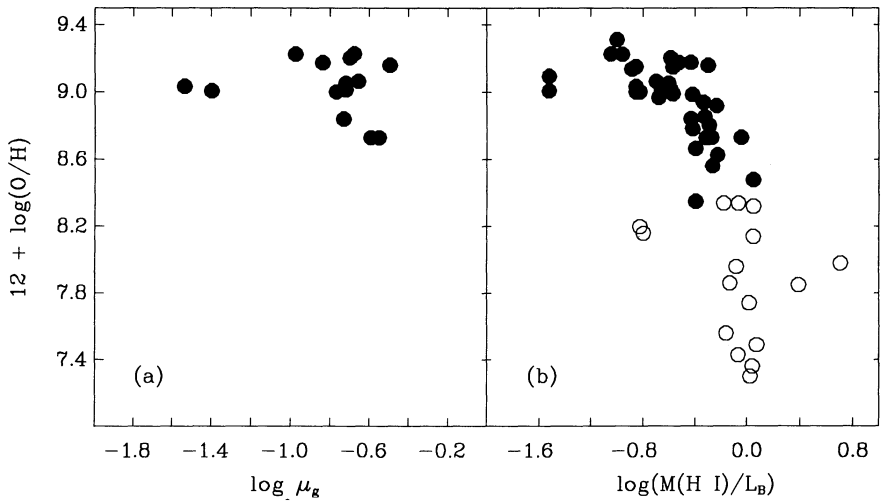

FIG. 14.—O/H plotted vs. gas fraction in the left panel (*a*) and vs. the galaxy's mass in H I divided by its blue luminosity (in solar units) in the right panel (*b*). Filled circles indicate our abundance data for galaxies for which the gas data was available in the literature. Open circles represent data from Skillman et al. (1989).

shown in Figure 11 shows no additional correlation with H I content once the $\bar{z}$ versus V_C correlation is removed. On the other hand, VE have found evidence that abundance correlates with molecular gas fraction (surface density of H_2/surface gas density). As VE note, the CO to H_2 conversions and other uncertainties in assessing the various gaseous components render any but the most fundamental conclusions suspect. Nevertheless, these weak correlations do offer possible physical explanations for a $\bar{z}$-T correlation. Whether they are the actual mechanisms for the observed $\bar{z}$-T or $\bar{z}$-L relations remains ambiguous. It is curious that elliptical galaxies share nearly the same $\bar{z}$-M_B relation as spirals and irregulars, yet in that case present-day gas fraction is clearly an irrelevant factor.

With the current data we are unable to resolve empirically whether mass or Hubble type is the primary underlying factor in determining $\bar{z}$. But what would such correlations mean? Consider an overdense region at high redshift that will become one of the galaxies in our sample. Its principal global characteristics are its mass, its environment, and the degree of internal structure. Somehow the initial properties of that overdense region are related via its evolution to the Hubble type of the final galaxy. Mass is the only current "observable" that is directly connected to the properties of the initial overdense region. Hubble type is presumably some indirect measure of the primordial environment (i.e., local density or nearest neighbor) and the level of initial substructure. The initial conditions plus subsequent evolution that determine Hubble type also determine gas fraction, bulge-to-disk ratio and possibly $\bar{z}$. A strong correlation between $\bar{z}$ and Hubble type would suggest that chemical evolution is determined in part by environment and/or initial structure, probably through their effects on the star formation history and IMF. On the other hand, if the correlation between $\bar{z}$ and V_C is stronger than the dependence on morphological type, that would suggest that other processes such as galactic mass loss may be more important. With our current precision and sample size the importance of galaxy mass and type are nearly comparable, so we cannot test whether environment or substructure affect $\bar{z}$. Finally, it is worth noting that the observed correlations of $\bar{z}$ with mass and type suggest that stochastic effects, such as starbursta and accretion events, probably do not seriously affect the global abundances of most galaxies. Interestingly, stochastic effects also seem to have negligible influence on the Tully-Fisher and Faber-Jackson relationships.

4.2.2. *Abundance Gradients and Galaxy Properties*

Searle (1971) and Shields (1974) concluded that the gradient in the [O III]/Hβ ratio was primarily, although not necessarily entirely, produced by nebular abundance gradients. This conclusion was confirmed by observations of high-excitation regions in the outer disks of galaxies (Searle & Sargent 1972; Smith 1975). However, these investigators also discussed other possible causes of the variation in emission-line ratios, such as variations in the dust-to-gas ratio and in stellar temperature. Our data confirm previous results that the gradient in [O III]/Hβ is not entirely accounted for by changing nebular elemental abundances (see Shields & Tinsley 1976, Shields & Searle 1978; Vílchez & Pagel 1988), but is at least in part due to changes in T_*. The emission-line gradient would still be entirely related to a metallicity gradient if T_* depends directly on abundance. For example, Talent (1980) proposed that $T_* \propto Z^{-0.17}$. Such a relationship might arise from increased line blanketing (Talent 1980), from a lower high-mass cutoff in the initial mass function (Viallefond 1985), or from metallicity effects on stellar evolution. However, changes in the ionizing spectra do not necessarily reflect changes in abundance. The change in the ratio of O to B stars across the disk could for example be a reflection of dynamically induced variations in the IMF (related to cloud-cloud collision rates, relative cloud velocities, shear, etc.). From existing studies it is generally accepted that radial gradients in the line ratios primarily reflect abundance gradients.

In contrast to the behavior of $\bar{z}$, the abundance gradients appear at best only weakly correlated with macroscopic quantities (see Table 4). We do not find statistically significant evidence for correlations between G and either V_C or T when the gradients are expressed in units of dex/ρ_0 or dex/ρ_s, regardless of whether barred galaxies are removed from the sample. However, the scatter among measured slopes is about twice as large as that expected from measurement uncertainties, which indicates that there is real variation among gradients. G does correlate with V_C when gradients are defined in terms of physical radius (kpc), mainly because more massive galaxies have larger isophotal radii.

The dependence of variations in G on the choice of radial normalization becomes apparent when considering the physical processes that might affect gradients. A small galaxy is unlikely to retain a steep gradient because it would quickly diffuse. On the other hand, a large galaxy is unlikely to be able to erase a steep gradient if one forms. The small galaxy is therefore less likely to have a large gradient in dex/isophotal radius, but it may have a very similar gradient to that of a large galaxy when expressed in dex/kpc. Whether G correlates with mass or Hubble type then depends on the choice of radial scaling and the correlation between isophotal radius and mass or Hubble type.

Some previous studies have claimed correlations between the gradients and either ρ_e (effective radius; Díaz 1989), M_B (Zaritsky, Elston, & Hill 1990), or Hubble type (VE and OK) while others have argued that no correlations exist (Belley & Roy 1992). Some of this difference in interpretation can be attributed to different definitions of G. VE focused on gradients in units of dex/kpc, OK found the most significant correlations for gradients expressed in units of dex/ρ_s, and we have concentrated on the gradients in units of dex/ρ_0. In Figure 15 we compare our data with that presented by VE for gradients expressed both in terms of dex/ρ_0 and dex/kpc. As with VE, we differentiate between barred and unbarred galaxies (VE also classified mixed types). The only correlation between G and T with greater than 95% confidence (2 σ) is in Figure 15*a* (VE's data for G expressed in terms of dex/kpc). If only one galaxy in our data (Fig. 15*c*) is rejected (either NGC 55 or NGC 3344), then our data would also show a significant correlation between G and T, when G is expressed in units of dex/kpc. Neither our data nor VE's shows a significant correlation between G and T, when G is expressed in terms of dex/ρ_0. This suggests that most of the observed type dependence of abundance gradients may be due to a disk size dependence, which correlates generally with type (cf. Fig. 11). Whether one observes a correlation between G and T depends on the normalization radius that is used.

Although we observe no correlation between G, in units of dex/ρ_0, and T, the relationship between G and T may be more complex than a simple correlation. Irregulars and other late-type galaxies might have shallow gradients because their size is close to a mixing length. Early types may have shallow gradients because they have exhausted the large majority of their gas and so have abundances that are near the yield throughout the galaxy. If this is the case only intermediate-type galaxies would then be expected to have steep gradients. There is some indication of such a relationship in Figure 15*d*, although clearly not a definitive one.

We see some evidence for a correlation with bar type, as has been claimed by Pagel & Edmunds (1981), VE, Martin (1992), and Edmunds & Roy (1993), regardless of which normalization radius is used. Classification varies among different sources, so we carefully examined available images of each galaxy and made our own designation when sources differed. We believe there are seven barred galaxies in our sample [NGC 55 (peculiar), NGC 925, NGC 1313, NGC 1365, NGC 3319, NGC 3351, and NGC 5236]. NGC 55 is seen edge-on and is asymmetric, so possibly it should not be included in this discussion. The other six galaxies are clearer cases and five of these, NGC 925, NGC 1313, NGC 1365, NGC 3351, and NGC 5236, have very shallow gradients (-0.256, -0.288, -0.188, -0.228, and -0.194, respectively, in units of dex/ρ_0). The average gradient for the entire sample is -0.59 dex/ρ_0. NGC 3319 has a measured gradient of -0.573, but a more careful look at the data (see Fig. 8) reveals that beyond $\rho_0 \sim 0.4$ the abundances are nearly constant. This may be a galaxy that is not characterized by a single exponential gradient (see discussion below). These results are not created by an observational bias because the radial range over which H II regions were observed are similar for the barred and unbarred galaxies. We examined whether

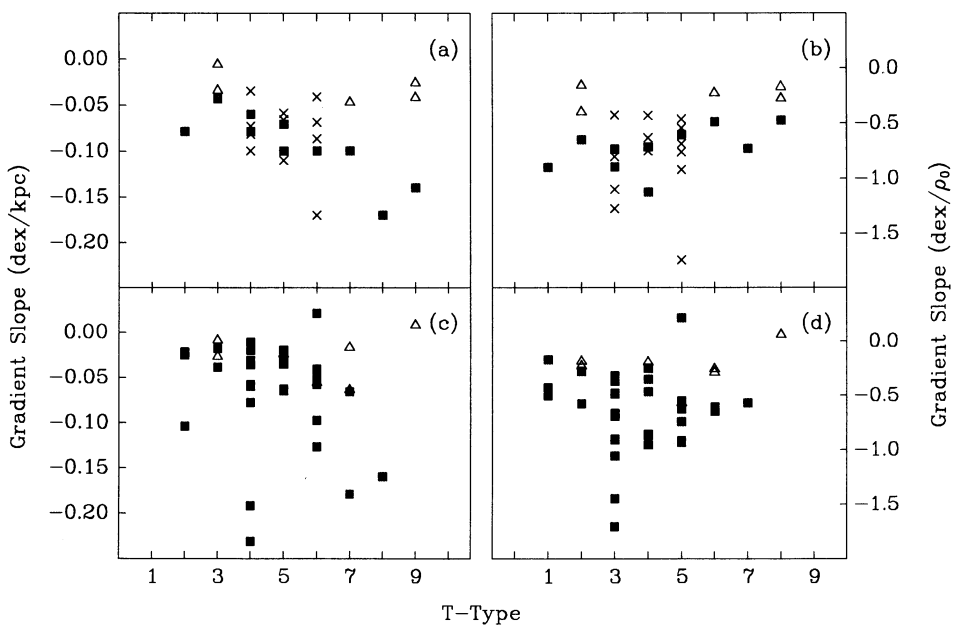

FIG. 15.—Comparison of abundance gradient data between our data and that of VE. Hubble type is expressed in units of T-type. Panels (*a*) and (*c*) contain gradient data in units of dex/kpc. Panels (*b*) and (*d*) contain gradient data in units of dex/isophotal radius. Panels (*a*) and (*b*) present VE's data. Panels (*c*) and (*d*) present our data. Barred galaxies are designated by open triangles, mixed types by crosses, and unbarred galaxies by solid squares.

there are significant differences in the abundance behavior across the bar radius. Only NGC 3319 shows any evidence for different behavior interior to the bar radius ($\rho/\rho_0 = 0.25$) than exterior to it. The gradient is apparently steeper in the bar region than outside. Overall, we find a strong indication that barred galaxies do have flatter gradients than unbarred galaxies. However, a few unbarred galaxies (e.g., NGC 253, NGC 2541, NGC 4321, NGC 5194, and NGC 7793) also have gradients that are significantly shallower than the average (-0.251, 0.216, -0.320, -0.370, and -0.369, respectively), and some barred galaxies have been shown to have normal gradients (NGC 4303; Martin & Roy 1992). The abundance distribution in NGC 2541 is particularly odd.

4.2.3. *Are Abundance Gradients Exponential?*

We have assumed that the variation in the logarithm of abundance with radius can be characterized by a straight line. Only with measurements of many H II region abundances per galaxy can we test this assumption. Vílchez et al. (1988) found that the gradient in M33 steepens significantly in the inner region of the disk. Similar bends in gradients were found in M101 (Zaritsky et al. 1990; Scowen et al. 1992), in the M81 data presented by Garnett & Shields (1987; see also Zaritsky 1992), and in NGC 300, NGC 5194, NGC 5457, and NGC 7793 (VE). This phenomenon is more clearly illustrated in the large databases like those compiled and presented by Zaritsky et al. and Scowen et al., rather than in Figure 8 which has fewer data per galaxy.

We remain concerned that the steepening of the line ratio gradient may not reflect a corresponding bend in the abundance. Such would be the case if there are strong nonlinearities in the abundance calibration of R_{23}. There is evidence that at metallicities above solar, R_{23} may become very sensitive to the density (OK). However, the steepening of the line ratio gradients does not appear to be caused by a strong nonlinearity in R_{23}. There are several galaxies in our sample (e.g., NGC 2403, NGC 2903, NGC 3344) that have gradients that do not show a corresponding steepening at abundances similar to those where the steepening is seen in other galaxies. Furthermore, the calculated abundance at which the steepening occurs varies among those galaxies that exhibit the phenomenon. However, these results may remain controversial until electron temperatures are measured for a significant number of regions in both the steep and shallow gradient regions.

Both Wyse & Silk (1989) and Zaritsky (1992) have proposed models that explain this steepening. Zaritsky (1992) studied the five galaxies that at the time had at least 15 observed H II regions from a single study. In the course of this work, we have found two other galaxies that have more than 15 observed H II regions (NGC 300 and NGC 7793). Neither of these has a dramatic bend in the gradient, although VE has claimed that both of these do show a bend. Using the technique described by Zaritsky (1992) to determine whether a single scale-length exponential provides an adequate fit, or whether two exponentials are necessary, we determined that both galaxies are adequately described by a single scale-length exponential. NGC 3319 and NGC 5033, two galaxies in the sample with fewer than 15 observed H II regions, show preliminary signs of a bend in their abundance gradient and merit further study. While the cause of any bend in the gradient remains an open question, we conclude that the abundance gradients in some galaxies are described well by a single exponential and others are definitely not. This should be considered when discussing properties of abundance gradients.

5. SUMMARY

We have presented results from a study of the oxygen abundance of H II regions in spiral galaxies, based on our own observations of 159 H II regions and data collected from the literature for about 400 other H II regions. First, we examined the observed line ratios of regions and briefly discussed implications for the physical parameters of those regions. We found in accordance with earlier studies that collisional effects on line strengths are generally unimportant. We also confirm the findings of Vílchez & Pagel (1988) that the η parameter generally increases with decreasing radius. This is best interpreted as an increase in the hardness of the ionizing radiation, which is expressed as an increase in the effective temperature, with increasing radius. This indicates that at least part of the gradient in [O III]/Hβ is not just due to changes in the nebular abundance. Extinction varies considerably from object to object in our sample, but it shows no systematic dependence on galactocentric radius or excitation.

We used the sample of 39 spiral galaxies, each with at least five observed H II regions, to examine possible relationships between the abundance and abundance gradient with the macroscopic properties of the galaxies. We found a strong correlation between abundance ($\bar{z}$) and the disk circular velocity (V_C). The relationship between $\bar{z}$ and absolute blue magnitude (M_B) is slightly weaker, presumably due to differences among mass-to-light ratios. We compared the relationship found for giant spirals with that found earlier for irregulars, ellipticals, and Local Group dE's, and found that these three samples of galaxies lie along well defined tracks in the M_B-abundance plane. Abundance also correlated strongly with Hubble type. Somewhat surprisingly, we find little correlation between $\bar{z}$ and the mean gas fraction of the disk. The question of which correlation is most significant is muddied by correlations between Hubble type and V_C. We concluded by discussing our expectations for the relative strengths of the various correlations resulting from very simple considerations of the evolution of galaxies.

We examined the abundance gradients for galaxies in the sample and found no correlations between the slope of the gradient and Hubble type or V_C for abundance gradients defined in units of dex/isophotal radius. However, results are not necessarily in conflict with previous claims of correlations because we cannot reject the hypothesis that both early and very late type spirals have gradients that are shallower than intermediate type spirals. We do find a correlation between the slope of the abundance gradient and T when the abundance gradient is expressed in terms of dex/kpc (in agreement with the results of VE). We identify a strong tendency for barred galaxies to have shallower gradients than unbarred galaxies, thereby confirming the earlier suggestion of Pagel & Edmunds (1981). The question of the shape of the abundance gradient remains open and awaits studies utilizing many observed regions per galaxy, at least 15 regions, and a better understanding of R_{23}.

Both the number of regions per galaxy and the number of galaxies observed is now sufficiently large to begin confidently to address simple questions regarding correlations between abundance and other properties of spiral galaxies. These correlations provide indirect, but measurable, clues to the nature of galaxy formation and evolution.

The authors thank R. Bender, D. Burstein, and S. Faber for providing data before publication and D. Garnett, G. Shields,

and E. Skillman for detailed comments on an earlier version of this manuscript. We also thank V. McIntyre for drawing our attention to an error in an earlier draft. D. Z. acknowledges financial support from NSF grant AST 88-22297 while at Steward Observatory, and from NASA through grant HF-1027.01-91A from STScI, which is operated by AURA, Inc. under NASA contract NAS 5-26555, while at the Carnegie Observatories. R. C. K. acknowledges funding from NSF grant AST 90-19150. J. P. H. acknowledges funding from NASA HST grant GO 2227.08-87A. Finally, the authors thank the telescope operators at the MMT (Carol Heller, John McAfee, Janet Robertson) and Steward 2.3 m (Dennis Means, Gary Rosenbaum) for their careful assistance.

REFERENCES

Aaronson, M. 1986, in Stellar Populations, ed. C. A. Norman, A. Renzini, & M. Tosi (Cambridge: Cambridge Univ. Press), 45
Belley, J., & Roy, J.-R. 1992, ApJS, 78, 61
Bender, R. 1992, in IAU Symp. 147, The Stellar Populations of Galaxies, ed. B. Barbuy & A. Renzini (Dordrecht: Reidel), 267
Bender, R., Burstein, D., & Faber, S. 1992, ApJ, 399, 462
———. 1993, ApJ, 411, 153
Blair, W. P., Kirshner, R. P., & Chevalier, R. A. 1982, ApJ, 254, 50
Brodie, J. P., & Huchra, J. P. 1991, ApJ, 379, 157
Boroson, T. 1981, ApJS, 46, 177
Boroson, T. A., Strom, K. M., & Strom, S. E. 1983, ApJ, 274, 39
Carignan, C. 1985, ApJS, 58, 107
Czyzak, S. J., Keyes, C. D., & Aller, L. H. 1986, ApJS, 61, 159
Deharveng, L., Caplan, J., Lequeux, J., Azzopardi, M., Breysacher, J., Tarenghi, M., & Westerlind, B. 1988, A&AS, 73, 407
Dennefeld, M., & Kunth, D. 1981, AJ, 86, 989
de Vaucouleurs, G., de Vaucouleurs, A., & Corwin, H. G. 1976, Second Reference Catalogue of Bright Galaxies (Austin: Univ. Texas Press), 1977 (RC2)
Díaz, A. I. 1989, in Evolutionary Phenomena in Galaxies, ed. J. E. Beckman & B. E. J. Pagel (Cambridge: Cambridge Univ. Press), 377
Díaz, A. I., Terlevich, E., Vílchez, J. M., Pagel, B. E. J., & Edmunds, M. G. 1991, MNRAS, 253, 245
Djorgovski, S., & Davis, M. 1987, ApJ, 313, 59
Dressler, A., Lynden-Bell, D., Burstein, D., Davies, R. L., Faber, S. M., Terlevich, R. J., & Wagner, G. 1987, ApJ, 313, 42
Dopita, M. A., & Evans, I. N. 1986, ApJ, 307, 431
Dufour, R. J., Talbot, R. J., Jensen, E. B., & Shields, G. A. 1980, ApJ, 236, 119
Edmunds, M. G., & Pagel, B. E. J. 1984, MNRAS, 211, 507 (EP)
Edmunds, M. G., & Roy, J.-R. 1993, MNRAS, 261, 17P
Elmegreen, B. G., & Elmegreen, D. M. 1985, ApJ, 288, 438
Elmegreen, D. M., & Elmegreen, B. G. 1984, ApJS, 54, 127
Evans, I. N., & Dopita, M. A. 1985, ApJS, 58, 125
Faber, S. M. 1973, ApJ, 179, 423
Franx, M., & Illingworth, G. 1990, ApJ, 359, L41
Garnett, D. R. 1989, ApJ, 345, 282
Garnett, D. R., & Shields, G. A. 1987, ApJ, 317, 82
Hawley, S. A., & Phillips, M. M. 1980, ApJ, 235, 783
Hayes, D. S., & Latham, D. W. 1975, ApJ, 197, 593
Heckman, T. M., Armus, L., & Miley, G. K. 1990, ApJS, 74, 833
Henry, R. B. C., Pagel, B. E. J., Lasseter, D. F., & Chincarini, G. K. 1992, MNRAS, 258, 321
Hodge, P. W. 1971, ARA&A, 9, 35
Huchtmeier, W. K., & Richter, O.-G. 1989, H I Observations of Galaxies (New York: Springer)
Kennicutt, R. C., Jr., Keel, W. C., & Blaha, C. A. 1989, AJ, 97, 1022
Kennicutt, R. C., Jr., & Martin, C. L. 1983, in preparation
Kent, S. M. 1987, AJ, 93, 817
Kodaira, K., Watanabe, M., & Okamura, S. 1986, ApJS, 62, 703
Kwitter, K. B., & Aller, L. H. 1981, MNRAS, 195, 939
Martin, P. 1992, Ph.D. thesis, Univ. Laval
Martin, P., & Roy, J.-R. 1992, ApJ, 397, 463
Mathis, J. S. 1982, ApJ, 261, 195
———. 1985, ApJ, 291, 247
McCall, M. L., Rybski, P. M., & Shields, G. A. 1985, ApJS, 57, 1 (MRS)
McGaugh, S. S. 1991, ApJ, 380, 140
Mendoza, C., & Zeippen, C. J. 1982, MNRAS, 198, 127
Mould, J. R. 1984, PASP, 96, 773
Nussbaumer, H., & Storey, P. J. 1981, A&A, 99, 177
Oey, M. S., & Kennicutt, R. C., Jr. 1993, ApJ, 411, 137 (OK)
Osterbrock, D. E. 1989, The Astrophysics of Gaseous Nebulae and Active Galactic Nuclei (Mill Valley, CA: University Science Books)
Pagel, B. E. J., & Edmunds, M. G. 1981, ARA&A, 2, 77
Pagel, B. E. J., Edmunds, M. G., Blackwell, D. E., Chun, M. S., & Smith, G. 1979, MNRAS, 189, 95
Pagel, B. E. J., Edmunds, M. G., Fosbury, R. A. E., & Webster, B. L. 1978, MNRAS, 184, 569
Pagel, B. E. J., Edmunds, M. G., & Smith, G. 1980, MNRAS, 193, 219
Rayo, J. F., Peimbert, M., & Torres-Peimbert, S. 1982, ApJ, 255, 1
Rieke, G. H., Lebofsky, M. J., Thompson, R. I., Low, F. J., & Tokunaga, A. T. 1980, ApJ, 238, 24
Sarazin, C. L. 1976, ApJ, 208, 323
Schild, R. E. 1977, AJ, 82, 337
Scowen, P. A., Dufour, R. J., & Hester, J. J. 1992, AJ, 104, 92
Searle, L. 1971, ApJ, 168, 327
Searle, L., & Sargent, W. L. W. 1972, ApJ, 173, 25
Shields, G. A. 1974, ApJ, 193, 335
Shields, G. A., & Searle, L. 1978, ApJ, 222, 821
Shields, G. A., Skillman, E. D., & Kennicutt, R. C., Jr. 1991, ApJ, 371, 82
Shields, G. A., & Tinsley, B. M. 1976, ApJ, 203, 66
Simien, F., & de Vaucouleurs, G. 1986, ApJ, 302, 564
Skillman, E. D., Kennicutt, R. C., Jr., & Hodge, P. W. 1989, ApJ, 347, 875
Smith, H. E. 1975, ApJ, 199, 591
Stauffer, J. R., & Bothun, G. D. 1984, AJ, 89, 1702
Talent, D. L. 1980, Ph.D. thesis, Rice University
Terlevich, R., Davies, R. L., Faber, S. M., & Burstein, D. 1981, MNRAS, 196, 381
Tully, R. B. 1988, Nearby Galaxies Catalog (Cambridge: Cambridge Univ. Press)
van der Hulst, J. M., Kennicutt, R. C., Crane, P. C., & Rots, A. H. 1988, A&A, 195, 38
Viallefond, F. 1985, in Star Forming Dwarf Galaxies and Related Objects, IAP Meeting No. 1 (Paris: Éditions Frontières), 207
Vila-Costas, M. B., & Edmunds, M. G. 1992, MNRAS, 259, 121 (VE)
Vílchez, J. M., & Pagel, B. E. J. 1988, MNRAS, 231, 257
Vílchez, J. M., Pagel, B. E. J., Díaz, A. I., Terlevich, E., & Edmunds, M. G. 1988, MNRAS, 235, 633
Walsh, J. R., & Roy, J.-R. 1989, ApJ, 341, 722
Webster, B. L., & Smith, M. G. 1983, MNRAS, 204, 743
Whitmore, B. C., & Kirshner, R. P. 1982, AJ, 87, 500
Wyse, R. F. G., & Silk, J. 1989, ApJ, 700, 339
Zaritsky, D. 1992, ApJ, 390, L73
Zaritsky, D., Elston, R., & Hill, J. M. 1990, AJ, 99, 1108